Available online at www.sciencedirect.com
ScienceDirect
Deep-Sea Research II 55 (2008) 638–652
DEEP-SEA RESEARCH PART II
www.elsevier.com/locate/dsr2

# Dissolved rare earth elements tracing lithogenic inputs over the Kerguelen Plateau (Southern Ocean)

Y. Zhang, F. Lacan, C. Jeandel*

*LEGOS (UMR5566), Université de Toulouse-CNRS-CNES-IRD, Observatoire Midi-Pyrénées, 14 av. Edouard Belin, 31400 Toulouse, France*

Accepted 16 December 2007

**Abstract**

Dissolved rare earth elements (REEs) were measured in the water masses upstream from and over the Kerguelen Plateau (Indian sector of the Southern Ocean). Upstream from the plateau, the REE profiles were consistent with published data from the Southern and Indian Oceans. Over the plateau (<500 m) the following features are observed: (1) higher REE concentrations at most stations, (2) weak Ce anomalies and HREE/LREE fractionations and (3) positive Eu anomalies similar to those of the Kerguelen and Heard basalts. This suggests that the high dissolved-REE contents observed in these waters result from the dissolution of lithogenic material from Kerguelen and/or Heard islands. REE pattern differences between the north and the south of the plateau suggest that both sources could be involved: Kerguelen Island influence in the north, through sporadic mesoscale intrusion of waters through the Polar Front, and Heard Island for the remaining stations, consistent with the main current direction over the Kerguelen Plateau.

A one-box model yields a lithogenic-Nd flux, from the dissolution of lithogenic material, of $89 \pm 20$ t Nd $y^{-1}$, and a corresponding dissolved-iron input larger than 100,000 t Fe $y^{-1}$. However, despite evidence of this significant lithogenic input, dissolved Fe is strongly depleted in the upper layers, contrasting with the enriched REE concentrations. This contrast stresses the different behaviours of REE and iron in the surface waters and the fact that strong fertilization does not imply dissolved Fe-replete waters.


*Keywords:* Rare earth elements; Seawater; Lithogenic input; Kerguelen Plateau; Eu anomaly; Natural fertilization

## 1. Introduction

The Southern Ocean is regarded as a key region in understanding the role of biogeochemical cycling on the variation of global climate (Marinov et al., 2006). Although this ocean is characterized by HNLC (high-nutrient low-chlorophyll) conditions, areas of high biomass do occur (De Baar et al., 1995; Moore et al., 2002) including the Kerguelen Plateau (Indian Sector of the Southern Ocean; Blain et al., 2008). These bloom occurrences are attributed to natural fertilization due to iron inputs from the Kerguelen archipelago and plateau (Blain et al., 2001). The major goal of the KEOPS project (KErguelen Ocean and Plateau compared Study program) was to study this natural iron fertilization, and in particular to identify its sources.

Oceanic iron has a lithogenic origin. It is a micronutrient required by phytoplankton for a variety of metabolic functions including nitrate utilization and chlorophyll production (Elrod et al., 2004). Dissolved Fe has two different oxidation states in seawater, Fe(III) and Fe(II). Fe(III) is the thermodynamically stable form in oxygenated waters. Studies suggest that 99% of dissolved iron is bound to organic ligands throughout the world's oceans, which maintains it dissolved and therefore bioavailable, by preventing the formation of iron hydroxides (Gledhill and Van den Berg, 1994; Rue and Bruland, 1997; Boye et al., 2001). The major dissolved iron sources to the upper ocean are thought to be the dissolution of atmospheric aerosols and sediment deposited on shelves and upper slopes (Johnson et al., 1999; Elrod et al., 2004).

Rare earth elements (REEs) in the ocean also have a lithogenic origin (Goldstein and Hemming, 2003). In some

*Corresponding author. Tel.: +33 561 332933; fax: +33 561 253205.
*E-mail addresses:* zhang@legos.obs-mip.fr (Y. Zhang), lacan@legos.obs-mip.fr (F. Lacan), catherine.jeandel@legos.obs-mip.fr (C. Jeandel).

0967-0645/$ - see front matter © 2008 Elsevier Ltd. All rights reserved.
doi:10.1016/j.dsr2.2007.12.029

cases, dissolved river loads and dissolution of aerosols can constitute significant dissolved REE sources (Tachikawa et al., 1999; Barroux et al., 2006). However, recent in situ and modelling studies suggest that dissolution of lithogenic sediments deposited on continental shelves and slopes is the dominant REE source to the ocean (Jeandel et al., 1998b; Lacan and Jeandel, 2001, 2005; Arsouze et al., 2007). REEs are an extremely coherent group in terms of chemical behaviour (Elderfield and Greaves, 1982). Despite this coherence, several processes cause slight fractionations within the group. These are displayed by shale-normalized REE patterns. Typical patterns of open-ocean waters display: (1) a heavy REE (HREE) enrichment relative to the light ones (LREE), mainly reflecting scavenging processes and (2) a depletion of Ce relative to its REE neighbours, reflecting the low solubility of this element when oxidized (Elderfield and Greaves, 1982; Bertram and Elderfield, 1993; Sholkovitz et al., 1994; German et al., 1995; Tachikawa et al., 1999). In some cases, specific features of the lithogenic source REE patterns allow tracing the lithogenic element origin in the ocean (Sholkovitz et al., 1999).

Although the Fe and REE oceanic cycles have some similarities (same origin, nutrient-like profiles) they mainly differ by the (i) the complex speciation of Fe and (ii) the fact that iron is taken up by biology. Dissolution of lithogenic material constitutes the main source for both dissolved Fe and REE in the ocean. We therefore propose here to use the REE concentrations in the Kerguelen Plateau waters to (i) trace the origin of the observed iron enrichment and (ii) quantify the fluxes of the lithogenic inputs. We present filtered seawater REE concentration profiles from nine stations upstream from and above the Kerguelen Plateau. The origins of the dissolved REE found above the plateau, the magnitude of the associated fluxes and the implications for the iron sources are discussed.

## 2. Sampling and method

### 2.1. Sampling

All the samples were collected during the KEOPS cruise, in austral summer (January–February 2005), on board the R/V *Marion Dufresne*. Three main transects, labelled A, B and C (Fig. 1), each composed of 11 stations, have been explored during the cruise. Each transect covered a wide range of depths from stations on the plateau (depths $<500$ m) to offshore stations ($500\,m<$ depths $<3500$ m). Station Kerfix, located upstream from the plateau is regarded as an "open-ocean" reference. Seawater samples (500 ml) from nine stations (A3, A11, B1, B5, B11, C1, C5, C11 and Kerfix, Fig. 1) were measured in this study. All the samples were collected using Niskin bottles mounted on a rosette frame equipped with a Sea-bird SBE-911 plus CTD sensor. The samples were filtered through Versapore 0.8 μm or Durapore 0.65 μm pore size filters, acidified to pH = 2 with twice-distilled HCl, stored at room temperature and transferred to the laboratory on land (LEGOS, Toulouse, France).

### 2.2. Analytical procedure

The purification and preconcentration of REE were performed following the method published by Tachikawa et al. (1999) and Lacan and Jeandel (2001). Briefly, the acidified seawater samples were spiked with $^{150}Nd$ and $^{172}Yb$. Then 2.5 mg Fe (dissolved $FeCl_3$) were added. After

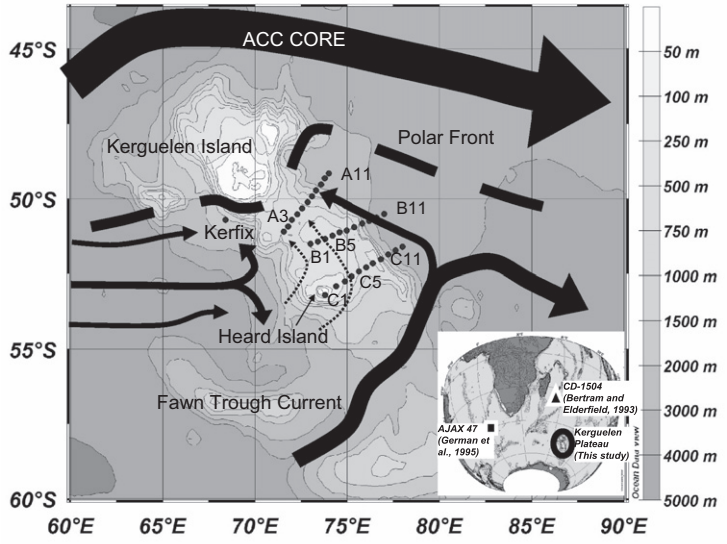


Fig. 1. Station locations of the KEOPS cruise discussed in this study. Station names are labelled. Main circulation features of the upper layer above the Kerguelen Plateau are given (Park et al., 2008a, b). Inset: Location of the Kerguelen Plateau in the Southern Ocean, and of the stations AJAX 47 (German et al., 1995) and CD-1504 (Bertram and Elderfield, 1993), where dissolved REE have been measured in previous studies.

isotopic equilibration for at least 24 h, the pH was increased to 7–8 by addition of $NH_4OH$, yielding REE–$Fe(OH)_3$ co-precipitation. The precipitate was extracted by centrifugation and rinsed three times with deionized water. An anion exchange column was used to purify the REE from the remaining matrix.

REE concentrations were then measured on a Perkin Elmer Elan 6000 Inductively Coupled Plasma Mass Spectrometer. All the REEs were determined by the external standard method, whereas Nd and Yb were additionally determined by isotopic dilution. Comparison of these two methods allowed us to determine the chemical procedure yields for Nd and Yb. They ranged between 80% and 100% for both elements. A linear interpolation relative to mass was then used to estimate the yields for the other REE.

We measured one blank in every 12 samples. The average blank values were less than 2% of the average signal (5% for the most depleted samples). The internal standard error was better than 5% ($2\sigma_n$) for all REEs on average (and equal to 10% for middle REE in the worst case). Four duplicate samples from station A3 (identified by their date, in Table 1) provide an estimate of the measurement reproducibility. For Nd and Yb determined by isotopic dilution, the mean relative deviation between duplicates was 2.6%. For the remaining REE, the mean relative deviation between duplicates was 5%, the highest value being 13%, excluding one outlier. Accuracy of the measurements was assessed by comparison of measurements of the SLRS4 certified reference material (riverine water, NRC Canada, not certified for REE) with a compilation of 174 measurements made by four independent laboratories (Yeghicheyan et al., 2001). The resulting accuracies were 0.8% for Nd, 6.5% for Yb and 5.6% on average for all the REE.

## 3. Hydrographic setting

### 3.1. Water masses

From surface to bottom, the following water masses were identified in the Kerguelen area (Park et al., 1998a, 2008a, b): relatively highly oxygenated Antarctic Surface Water (AASW, $O_2 > 7\,ml\,l^{-1}$), low-oxygenated upper circumpolar deep water (UCDW, from 200 to 1400 m, $O_2 < 4.5\,ml\,l^{-1}$), lower circumpolar deep water (1400 < LCDW < 2600 m) with its deep salinity maximum and the Antarctic bottom water (2600 m < AABW) only identifiable at the deeper stations B11 and C11 and characterized by lower temperature and salinity, whereas oxygen increases near the bottom. During the austral summer, the surface mixed layer (SML, ~80–100 m thickness) is constituted of relatively warm and fresh AASW, overlying the Winter Water (WW) characterized by a temperature minimum (−0.5 to +2.0 °C) and centred around 200 m (Park et al., 2008b). WW have been observed at every station except C1, which is a shallow station located in the close vicinity of Heard Island. However, hydrological characteristics of the WW vary widely indicating different origins for this specific water mass (Park et al., 2008b).

### 3.2. Circulation patterns and currents

Two principal current systems surround the Kerguelen Plateau (Fig. 1): the Antarctic Circumpolar Current (ACC) and the Fawn Trough Current (McCartney and Donohue, 2007; Park et al., 2008b). Most of the eastward flowing ACC transport (~100 Sv, $1\,Sv = 10^6\,m^3\,s^{-1}$) is deflected north of the Kerguelen Island, a residual fraction of ca. 30 Sv flow through the Antarctic Zone between Kerguelen and Antarctica (Park et al., 2008b). The Fawn Trough Current, originating from the eastern Enderby Basin (south of 58°S), bends to the north from 72°E to pass the Fawn Trough. A relatively strong northward branch of the Fawn Trough Current (up to $18\,cm\,s^{-1}$) transports cold Antarctic waters of southeastern Enderby Basin origin along the eastern flank of the plateau (Fig. 1). The core of this branch flows east of transect C, although station C11 is likely affected by the current. It then flows across Section B, around station B9 (50°42′S, 76°12′E) and extends northwestward up to 50°S (Park et al., 2008b). Over the plateau, the geostrophic circulation is relatively sluggish ($3–5\,cm\,s^{-1}$) and directed to the northwest parallel to the local bathymetry (Park et al., 2008b). During KEOPS, all the stations were located south of the Polar Front (PF). They are likely separated from the direct influence of the Kerguelen Island by a strong jet, inducing a non-productive narrow band revealed by satellite images (Park et al., 1998a; Blain et al., 2007; Mongin et al., 2008). However, the intrinsic variability of the PF makes that the northernmost stations of KEOPS could have been sporadically influenced by the water masses flowing north of this front (Rosemary Morrow, personal communication). Based on Geostrophic Velocity Field analyses, Mongin et al. (2008) underline the occurrence of strong eddy activity within the meanders of the Sub-Antarctic front to the east of Kerguelen Island, and some penetration of eddies over the plateau. Estimated vertical eddy diffusivities ($3\,10^{-4}\,m^2\,s^{-1}$) at stations A3 and C11 are one order of magnitude higher than the classical open-ocean value ($0.1\,10^{-4}\,m^2\,s^{-1}$), suggesting possible transfer of bottom water into the surface mixed layer (Park et al., 2008a).

Station Kerfix is located 100 miles southwest off the Kerguelen Island coast and upstream from the plateau, under the main influence of the residual ACC fraction, south of the PF (Fig. 1; Jeandel et al., 1998a; Park et al., 1998b). This is a relatively quiet part of the ACC with a sluggish dynamic. These open-ocean characteristics are confirmed by recent $^{230}Th_{xs}$ results, displaying linear increase with depth, typical of an open-ocean station (Roy-Barman et al., 1996; Venchiarutti et al., 2008). All these characteristics led us to consider station Kerfix as the "open-ocean" reference station in this study.

Table 1
Dissolved rare earth element concentrations (pmol $kg^{-1}$) and hydrographlc properties of the water masses of the Kerguelen Plateau, together with the dissolved Fe data (Blain et al., 2008)

| Sample depth (m) | Pot. temp. (°C) | Salinity | Sigma ($kg\,m^{-3}$) | Oxygen ($ml\,l^{-1}$) | $NO_3$ ($\mu mol\,kg^{-1}$) | $PO_4$ ($\mu mol\,kg^{-1}$) | $SiO_2$ ($\mu mol\,kg^{-1}$) | La | Ce | Pr | Nd | Sm | Eu | Gd | Tb | Dy | Ho | Er | Tm | Yb | Lu | Ce/Ce* | 2σ | $(La/Yb)_n$ | 2σ | Eu/Eu* | 2σ | Water mass | Depth for Fe | Fe[a] ($nmol\,kg^{-1}$) |
|---|---|---|---|---|---|---|---|---|---|---|---|---|---|---|---|---|---|---|---|---|---|---|---|---|---|---|---|---|---|---|
| C1 (53°11.00′S 73°51.90′E; water depth, 131 m; 8 February 2005)[b] | | | | | | | | | | | | | | | | | | | | | | | | | | | | | | |
| 0 | 2.5446 | 33.9488 | 27.0856 | 7.2580 | 27.466 | 1.913 | 21.656 | 32.3 | 24.0 | 4.5 | 19.4 | 3.4 | 0.92 | 4.3 | 0.64 | 5.0 | 1.3 | 4.9 | 0.75 | 5.0 | 0.93 | 0.44 | 0.02 | 0.38 | 0.006 | 1.24 | 0.06 | AASW | 20 | 0.78 |
| 30 | 2.5372 | 33.9496 | 27.0869 | 7.2514 | 27.207 | 1.946 | 21.838 | 35.9 | 28.1 | 5.2 | 21.9 | 3.8 | 1.01 | 4.8 | 0.70 | 5.3 | 1.4 | 5.0 | 0.73 | 5.0 | 0.93 | 0.46 | 0.02 | 0.43 | 0.006 | 1.23 | 0.05 | AASW | 40 | 0.81 |
| 50 | 2.5426 | 33.9488 | 27.0857 | 7.2610 | 28.502 | 2.012 | 21.656 | 34.7 | 27.2 | 5.1 | 21.5 | 3.7 | 0.99 | 4.7 | 0.72 | 5.4 | 1.5 | 5.3 | 0.77 | 5.1 | 0.93 | 0.46 | 0.02 | 0.40 | 0.007 | 1.21 | 0.06 | AASW | 80 | 0.78 |
| 100 | 2.4820 | 33.9564 | 27.0969 | 7.2231 | 28.243 | 1.979 | 21.838 | 32.5 | 23.9 | 4.7 | 19.5 | 3.5 | 0.89 | 4.5 | 0.66 | 5.2 | 1.4 | 5.3 | 0.75 | 5.3 | 0.91 | 0.43 | 0.02 | 0.37 | 0.005 | 1.16 | 0.06 | AASW | 120 | 0.81 |
| 130 | 2.4735 | 33.9578 | 27.0988 | 7.2173 | 29.020 | 2.111 | 22.566 | 31.5 | 22.4 | 4.6 | 18.9 | 3.1 | 0.85 | 4.4 | 0.66 | 5.2 | 1.4 | 5.3 | 0.78 | 5.4 | 0.92 | 0.42 | 0.01 | 0.35 | 0.007 | 1.17 | 0.06 | AASW | | |
| C5 (52°25.40′S 75°35.90′; water depth, 506 m; 7 February 2005)[b] | | | | | | | | | | | | | | | | | | | | | | | | | | | | | | |
| 0 | 2.7909 | 33.8839 | 27.0126 | 7.6037 | 26.002 | 2.197 | 14.294 | 19.7 | 4.04 | 2.4 | 10.9 | 1.8 | 0.47 | 3.1 | 0.50 | 4.2 | 1.3 | 4.6 | 0.68 | 4.8 | 0.85 | 0.13 | 0.01 | 0.22 | 0.001 | 1.01 | 0.04 | AASW | 40 | 0.063 |
| 30 | 2.7792 | 33.8847 | 27.0143 | 7.5465 | 26.384 | 1.982 | 14.387 | 20.9 | 3.3 | 2.4 | 10.8 | 1.9 | 0.50 | 3.1 | 0.50 | 4.3 | 1.3 | 4.7 | 0.70 | 4.7 | 0.84 | 0.10 | 0.01 | 0.27 | 0.001 | 1.03 | 0.03 | AASW | 80 | 0.071 |
| 50 | 2.6722 | 33.8867 | 27.0251 | 7.5393 | | | | 18.6 | 2.9 | 2.3 | 11.0 | 2.0 | 0.57 | 3.3 | 0.53 | 4.3 | 1.3 | 4.7 | 0.71 | 4.6 | 0.85 | 0.10 | 0.01 | 0.24 | 0.001 | 1.11 | 0.10 | AASW | 120 | 0.08 |
| 100 | 2.5103 | 33.8905 | 27.0418 | 7.4815 | 26.512 | 2.245 | 15.222 | 19.8 | 3.5 | 2.4 | 10.8 | 1.8 | 0.48 | 3.1 | 0.50 | 4.2 | 1.3 | 4.6 | 0.68 | 4.5 | 0.85 | 0.11 | 0.01 | 0.26 | 0.001 | 1.03 | 0.03 | AASW | 150 | 0.08 |
| 150 | 1.7306 | 33.9423 | 27.1446 | 7.3067 | 28.933 | 2.532 | 34.070 | 20.5 | 4.5 | 2.5 | 11.6 | 2.0 | 0.51 | 3.3 | 0.54 | 4.5 | 1.3 | 4.8 | 0.73 | 5.0 | 0.93 | 0.14 | 0.01 | 0.24 | 0.001 | 0.99 | 0.03 | WW | 200 | 0.26 |
| 200 | 1.5887 | 34.0495 | 27.2409 | 6.7121 | 32.885 | 2.795 | 44.390 | 22.8 | 8.8 | 3.1 | 13.4 | 2.3 | 0.59 | 3.4 | 0.56 | 4.5 | 1.3 | 4.8 | 0.71 | 4.9 | 0.89 | 0.24 | 0.02 | 0.28 | 0.003 | 1.05 | 0.04 | WW | 300 | 0.30 |
| 300 | 1.8348 | 34.1930 | 27.3378 | 5.7221 | | | | 22.2 | 5.6 | 2.8 | 12.5 | 2.1 | 0.55 | 3.3 | 0.56 | 4.6 | 1.4 | 4.9 | 0.75 | 5.0 | 0.95 | 0.16 | 0.01 | 0.26 | 0.001 | 1.03 | 0.04 | UCDW | 400 | 0.37 |
| 350 | 2.0752 | 34.2755 | 27.3853 | 5.1531 | | | | 23.9 | 6.5 | 2.9 | 12.9 | 2.2 | 0.57 | 3.4 | 0.56 | 4.7 | 1.4 | 4.9 | 0.77 | 5.3 | 0.97 | 0.17 | 0.01 | 0.22 | 0.001 | 1.02 | 0.03 | UCDW | 450 | 0.52 |
| 400 | 2.1911 | 34.3506 | 27.4362 | 4.7699 | 36.199 | 3.011 | 67.970 | 23.9 | 5.0 | 2.8 | 12.3 | 2.1 | 0.55 | 3.5 | 0.58 | 4.8 | 1.5 | 5.1 | 0.80 | 5.4 | 1.03 | 0.14 | 0.01 | 0.26 | 0.001 | 0.98 | 0.03 | UCDW | 500 | 0.58 |
| 450 | 2.0823 | 34.4000 | 27.4845 | 4.9164 | | | | 23.9 | 8.3 | 3.3 | 14.2 | 2.3 | 0.62 | 3.7 | 0.59 | 5.0 | 1.4 | 5.0 | 0.78 | 5.3 | 1.00 | 0.14 | 0.01 | 0.20 | 0.002 | 1.06 | 0.03 | UCDW | | |
| 500 | 2.0835 | 34.4297 | 27.5082 | 4.8263 | 34.287 | 3.083 | 71.790 | 22.1 | 7.0 | 3.0 | 14.2 | 2.2 | 0.60 | 3.4 | 0.58 | 4.9 | 1.4 | 5.1 | 0.80 | 6.0 | 1.03 | 0.19 | 0.02 | 0.22 | 0.002 | 1.07 | 0.04 | UCDW | | |
| C11 (51°38.48′S 77°59.61′E; water depth, 3224 m; 28 January 2005) | | | | | | | | | | | | | | | | | | | | | | | | | | | | | | |
| 0 | 1.7511 | 33.8255 | 27.0495 | 7.5914 | 29.564 | 2.078 | 23.259 | 22.5 | 7.5 | 2.9 | 13.5 | 2.1 | 0.56 | 3.3 | 0.51 | 4.4 | 1.3 | 4.6 | 0.67 | 5.1 | 0.84 | 0.21 | 0.01 | 0.26 | 0.002 | 1.09 | 0.05 | AASW | 40 | 0.12 |
| 50 | 1.7418 | 33.8261 | 27.0506 | 7.6055 | | | | 21.9 | 3.2 | 2.8 | 12.8 | 2.3 | 0.64 | 3.8 | 0.57 | 4.9 | 1.4 | 5.2 | 0.77 | 5.2 | 0.90 | 0.09 | 0.01 | 0.25 | 0.001 | 1.12 | 0.05 | AASW | 60 | 0.13 |
| 150 | 0.2837 | 33.9805 | 27.2682 | 7.3972 | 33.921 | 2.235 | 47.895 | 23.7 | 3.4 | 2.9 | 13.5 | 2.4 | 0.63 | 3.7 | 0.58 | 4.8 | 1.4 | 5.0 | 0.73 | 5.1 | 0.9 | 0.09 | 0.01 | 0.27 | 0.001 | 1.07 | 0.07 | WW | 80 | 0.07 |
| 300 | 1.8284 | 34.3555 | 27.4686 | 4.7068 | | | | 24.2 | 3.1 | 2.9 | 13.5 | 2.4 | 0.65 | 3.9 | 0.62 | 5.0 | 1.4 | 5.5 | 0.77 | 5.8 | 1.0 | 0.08 | 0.01 | 0.25 | 0.001 | 1.06 | 0.06 | UCDW | 100 | 0.05 |
| 700 | 2.1551 | 34.6428 | 27.6731 | 3.9965 | | | | 28.1 | 4.1 | 3.5 | 15.6 | 2.7 | 0.70 | 4.1 | 0.66 | 5.3 | 1.5 | 5.4 | 0.83 | 5.7 | 1.0 | 0.09 | 0.01 | 0.29 | 0.001 | 1.07 | 0.04 | UCDW | 150 | 0.09 |
| 1000 | 2.0182 | 34.7205 | 27.7463 | 4.2162 | 36.411 | 2.887 | 91.670 | 31.6 | 5.0 | 3.8 | 17.6 | 3.1 | 0.86 | 4.9 | 0.75 | 5.8 | 1.7 | 6.0 | 0.90 | 6.3 | 1.1 | 0.10 | 0.01 | 0.28 | 0.001 | 1.14 | 0.06 | UCDW | 200 | 0.10 |
| 2000 | 1.3680 | 34.7450 | 27.8151 | 4.5859 | 34.543 | 2.887 | 94.245 | 40.0 | 4.4 | 4.9 | 21.6 | 3.9 | 1.01 | 5.6 | 0.87 | 6.6 | 1.8 | 6.5 | 0.95 | 6.9 | 1.2 | 0.07 | 0.01 | 0.34 | 0.001 | 1.10 | 0.04 | LCDW | 600 | 0.24 |
| 2800 | 0.7471 | 34.7159 | 27.8335 | 4.7178 | | | | 36.7 | 5.3 | 5.2 | 23.4 | 4.2 | 1.14 | 5.9 | 0.93 | 7.2 | 2.0 | 6.7 | 1.01 | 7.2 | 1.2 | 0.09 | 0.01 | 0.30 | 0.001 | 1.15 | 0.06 | LCDW | 800 | 0.27 |
| 3180 | 0.3250 | 34.6979 | 27.8444 | 4.9061 | 36.722 | 3.435 | 111.755 | 42.6 | 6.1 | 6.0 | 27.6 | 4.7 | 1.25 | 6.5 | 0.95 | 7.5 | 2.0 | 7.0 | 1.02 | 7.3 | 1.2 | 0.09 | 0.01 | 0.34 | 0.001 | 1.17 | 0.04 | AABW | 1000 | 0.27 |
| | | | | | | | | | | | | | | | | | | | | | | | | | | | | | 1500 | 0.38 |
| | | | | | | | | | | | | | | | | | | | | | | | | | | | | | 2500 | 0.36 |

Table 1 (*continued*)

| Sample depth (m) | Pot. temp. (°C) | Salinity | Sigma ($kg\,m^{-3}$) | Oxygen ($ml\,l^{-1}$) | $NO_3$ ($\mu mol\,kg^{-1}$) | $PO_4$ ($\mu mol\,kg^{-1}$) | $SiO_2$ ($\mu mol\,kg^{-1}$) | La | Ce | Pr | Nd | Sm | Eu | Gd | Tb | Dy | Ho | Er | Tm | Yb | Lu | Ce/Ce* | 2σ | $(La/Yb)_n$ | 2σ | Eu/Eu* | 2σ | Water mass | Depth for Fe | Fe[a] ($nmol\,kg^{-1}$) |
|---|---|---|---|---|---|---|---|---|---|---|---|---|---|---|---|---|---|---|---|---|---|---|---|---|---|---|---|---|---|---|
| B1 (51°29.54′S 73°00.29′E; water depth, 325 m; 2 February 2005) | | | | | | | | | | | | | | | | | | | | | | | | | | | | | | |
| 0 | 3.3565 | 33.8944 | 26.9698 | 7.4262 | 22.217 | | 2.617 | 20.7 | 8.6 | 2.9 | 12.4 | 2.0 | 0.54 | 3.2 | 0.5 | 4.1 | 1.2 | 4.4 | 0.66 | 4.51 | 0.81 | 0.25 | 0.01 | 0.24 | 0.002 | 1.07 | 0.03 | AASW | 40 | 0.085 |
| 20 | 3.3564 | 33.8946 | 28.9700 | 7.4336 | 21.936 | | 2.617 | 21.8 | 9.0 | 3.0 | 13.0 | 2.1 | 0.56 | 3.3 | 0.5 | 4.2 | 1.2 | 4.5 | 0.66 | 4.51 | 0.80 | 0.25 | 0.01 | 0.24 | 0.002 | 1.07 | 0.03 | AASW | 80 | 0.056 |
| 50 | 3.3508 | 33.8954 | 26.9712 | 7.4315 | 21.936 | 1.691 | 2.617 | 20.7 | 8.2 | 2.9 | 12.5 | 2.2 | 0.56 | 3.3 | 0.5 | 4.3 | 1.3 | 4.5 | 0.68 | 4.61 | 0.84 | 0.24 | 0.01 | 0.23 | 0.002 | 1.06 | 0.04 | AASW | 120 | 0.067 |
| 100 | 2.9088 | 33.9175 | 27.0291 | 7.2787 | 24.467 | 2.092 | 10.470 | 21.1 | 8.1 | 3.0 | 12.8 | 2.1 | 0.55 | 3.3 | 0.5 | 4.4 | 1.3 | 4.7 | 0.68 | 4.65 | 0.85 | 0.23 | 0.01 | 0.23 | 0.002 | 1.05 | 0.03 | AASW | 150 | 0.071 |
| 150 | 2.3025 | 33.9856 | 27.1350 | 6.8863 | 28.966 | 2.359 | 23.034 | 21.7 | 8.1 | 2.9 | 12.8 | 2.1 | 0.57 | 3.3 | 0.5 | 4.4 | 1.3 | 4.7 | 0.70 | 4.78 | 0.90 | 0.23 | 0.01 | 0.23 | 0.001 | 1.06 | 0.04 | WW | 250 | 0.16 |
| 200 | 2.0216 | 34.0729 | 27.2272 | 6.4012 | 30.373 | 2.459 | 47.440 | 22.3 | 7.2 | 2.9 | 13.2 | 2.1 | 0.55 | 3.4 | 0.5 | 4.6 | 1.3 | 4.8 | 0.73 | 5.0 | 0.9 | 0.20 | 0.01 | 0.27 | 0.001 | 1.03 | 0.03 | WW | 300 | 0.16 |
| 300 | 1.9955 | 34.1219 | 27.2685 | 6.1051 | 31.497 | 2.493 | 52.460 | 22.2 | 7.3 | 3.0 | 13.1 | 2.1 | 0.56 | 3.3 | 0.5 | 4.5 | 1.3 | 4.7 | 0.73 | 4.99 | 0.93 | 0.20 | 0.01 | 0.22 | 0.001 | 1.04 | 0.03 | UCDW | 350 | 0.20 |
| 350 | 2.0057 | 34.1587 | 27.2972 | 5.8723 | 32.341 | 2.793 | 59.460 | 22.9 | 7.4 | 3.0 | 13.1 | 2.2 | 0.56 | 3.4 | 0.6 | 4.6 | 1.4 | 4.8 | 0.74 | 5.14 | 0.96 | 0.20 | 0.01 | 0.22 | 0.001 | 1.03 | 0.03 | UCDW | | |
| B5 (51°06.10′S 74°35.90′E; water depth, 457 m; 30 January 2005) | | | | | | | | | | | | | | | | | | | | | | | | | | | | | | |
| 0 | 2.7875 | 33.9021 | 27.0275 | 7.6002 | 24.267 | 1.702 | 4.469 | 22.0 | 9.3 | 2.8 | 12.5 | 2.2 | 0.60 | 3.3 | 0.50 | 4.3 | 1.2 | 4.6 | 0.67 | 4.7 | 0.86 | 0.26 | 0.01 | 0.28 | 0.002 | 1.15 | 0.06 | AASW | 40 | 0.064 |
| 60 | 2.6728 | 33.9095 | 27.0433 | 7.5478 | 24.267 | 1.768 | 3.457 | 24.3 | 11.1 | 3.2 | 14.1 | 2.4 | 0.62 | 3.6 | 0.56 | 4.6 | 1.3 | 4.9 | 0.69 | 4.9 | 0.83 | 0.28 | 0.02 | 0.30 | 0.003 | 1.07 | 0.06 | AASW | 60 | 0.051 |
| 150 | 1.7266 | 34.0048 | 27.1950 | 6.9274 | 27.426 | 2.493 | 22.513 | 27.9 | 14.8 | 3.8 | 15.8 | 2.5 | 0.67 | 3.7 | 0.55 | 4.7 | 1.3 | 4.9 | 0.74 | 5.1 | 0.86 | 0.32 | 0.02 | 0.32 | 0.004 | 1.13 | 0.05 | WW | 120 | 0.055 |
| 250 | 1.8287 | 34.1174 | 27.2777 | 6.2586 | | | | 31.1 | 11.7 | 3.5 | 15.0 | 2.6 | 0.68 | 3.7 | 0.55 | 4.7 | 1.3 | 4.8 | 0.67 | 4.8 | 0.84 | 0.24 | 0.01 | 0.33 | 0.003 | 1.13 | 0.05 | UCDW | 150 | 0.087 |
| 350 | 2.0850 | 34.3366 | 27.4335 | 4.9977 | | | | 25.8 | 8.6 | 3.3 | 14.2 | 2.4 | 0.65 | 3.6 | 0.54 | 4.6 | 1.3 | 4.9 | 0.72 | 5.1 | 0.89 | 0.21 | 0.01 | 0.28 | 0.002 | 1.13 | 0.05 | UCDW | 200 | 0.087 |
| 450 | 2.1293 | 34.4318 | 27.5062 | 4.6749 | 36.031 | 2.723 | 81.037 | 24.2 | 8.0 | 3.2 | 14.5 | 2.6 | 0.71 | 3.8 | 0.62 | 4.9 | 1.5 | 5.1 | 0.80 | 5.5 | 0.99 | 0.20 | 0.01 | 0.26 | 0.003 | 1.12 | 0.08 | UCDW | 300 | 0.18 |
| B11 (50°30.14′S 76°59.88′E; water depth, 3196 m; 29 January 2005) | | | | | | | | | | | | | | | | | | | | | | | | | | | | | | |
| 0 | 2.1170 | 33.8064 | 27.0064 | 7.5971 | 29.758 | 2.280 | 23.058 | 28.4 | 7.5 | 3.3 | 14.4 | 2.3 | 0.63 | 3.6 | 0.55 | 4.8 | 1.4 | 5.1 | 0.73 | 5.1 | 0.88 | 0.17 | 0.01 | 0.33 | 0.002 | 1.13 | 0.05 | AASW | | |
| 50 | 2.0866 | 33.8062 | 27.0086 | 7.5839 | 29.499 | 2.111 | 23.058 | 23.5 | 3.5 | 2.9 | 13.2 | 2.3 | 0.62 | 3.7 | 0.6 | 4.9 | 1.3 | 5.1 | 0.73 | 5.1 | 0.88 | 0.09 | 0.01 | 0.26 | 0.001 | 1.08 | 0.06 | AASW | | |
| 100 | 0.8583 | 33.8452 | 27.1259 | 7.6756 | 30.017 | 2.179 | 24.381 | 21.8 | 3.2 | 2.8 | 12.8 | 2.3 | 0.62 | 3.6 | 0.6 | 4.7 | 1.4 | 5.0 | 0.73 | 5.1 | 0.89 | 0.09 | 0.01 | 0.24 | 0.001 | 1.08 | 0.08 | AASW | | |
| 150 | −0.1582 | 34.0141 | 27.3182 | 7.2294 | 32.604 | 2.549 | 49.507 | 22.9 | 3.0 | 2.9 | 13.2 | 2.3 | 0.65 | 3.7 | 0.6 | 4.9 | 1.4 | 5.0 | 0.74 | 5.2 | 0.93 | 0.08 | 0.01 | 0.24 | 0.001 | 1.16 | 0.06 | WW | | |
| 300 | 2.0887 | 34.4070 | 27.4896 | 4.3751 | | | | 22.3 | 3.0 | 2.8 | 12.4 | 2.2 | 0.58 | 3.5 | 0.5 | 4.8 | 1.4 | 5.1 | 0.75 | 5.4 | 0.97 | 0.08 | 0.01 | 0.24 | 0.001 | 1.06 | 0.05 | UCDW | | |
| 700 | 2.1692 | 34.6418 | 27.6711 | 4.0040 | | | | 25.8 | 3.8 | 3.2 | 14.3 | 2.8 | 0.76 | 4.3 | 0.7 | 5.4 | 1.5 | 5.6 | 0.82 | 5.9 | 1.07 | 0.09 | 0.01 | 0.24 | 0.001 | 1.12 | 0.06 | UCDW | | |
| 1000 | 2.0663 | 34.7078 | 27.7323 | 4.1649 | 36.874 | 3.088 | 94.000 | 26.8 | 3.9 | 3.5 | 15.9 | 2.9 | 0.82 | 4.5 | 0.7 | 5.8 | 1.6 | 5.9 | 0.90 | 6.2 | 1.17 | 0.09 | 0.01 | 0.24 | 0.001 | 1.13 | 0.05 | UCDW | | |
| 2000 | 1.2938 | 34.7421 | 27.8180 | 4.5968 | 34.933 | 2.869 | 108.084 | 30.0 | 4.3 | 4.3 | 19.2 | 3.5 | 0.90 | 5.0 | 0.8 | 5.9 | 1.6 | 5.6 | 0.90 | 5.9 | 1.10 | 0.09 | 0.01 | 0.30 | 0.001 | 1.09 | 0.08 | LCDW | | |
| 2800 | 0.4639 | 34.7037 | 27.8398 | 4.7983 | 35.968 | 2.954 | 117.425 | 40.5 | 5.5 | 5.7 | 25.3 | 4.6 | 1.18 | 6.5 | 1.0 | 7.5 | 2.0 | 7.0 | 1.07 | 7.5 | 1.37 | 0.08 | 0.01 | 0.32 | 0.001 | 1.11 | 0.05 | LCDW | | |
| 3146 | 0.1166 | 34.6885 | 27.8485 | 4.9824 | 37.003 | 3.156 | 127.941 | 41.5 | 6.2 | 6.0 | 26.2 | 4.7 | 1.20 | 6.5 | 1.0 | 7.5 | 2.0 | 7.0 | 1.05 | 7.3 | 1.34 | 0.09 | 0.01 | 0.34 | 0.001 | 1.09 | 0.05 | AABW | | |
| A3 (50°42.32′S 71°59.83′E; water depth, 482 m; 24 January 2005) | | | | | | | | | | | | | | | | | | | | | | | | | | | | | | |
| 0 | 3.6525 | 33.9002 | 26.9461 | 7.5301 | | | | 23.3 | 8.8 | 3.1 | 13.4 | 2.4 | 0.69 | 3.6 | 0.56 | 4.5 | 1.3 | 4.7 | 0.70 | 4.6 | 0.84 | 0.23 | 0.01 | 0.30 | 0.003 | 1.20 | 0.05 | AASW | 20 | 0.075 |
| 20 | 3.6503 | 33.9008 | 26.9467 | 7.5290 | 23.018 | 1.581 | 1.581 | 23.5 | 8.6 | 3.1 | 13.9 | 2.4 | 0.71 | 3.6 | 0.57 | 4.5 | 1.3 | 4.8 | 0.70 | 4.7 | 0.83 | 0.22 | 0.01 | 0.30 | 0.002 | 1.22 | 0.06 | AASW | 60 | 0.069 |
| 50 | 3.5358 | 33.9015 | 28.9584 | 7.5018 | | | | 23.6 | 9.3 | 3.2 | 13.9 | 2.4 | 0.76 | 3.7 | 0.57 | 4.7 | 1.4 | 4.8 | 0.71 | 4.8 | 0.87 | 0.24 | 0.01 | 0.29 | 0.002 | 1.29 | 0.06 | AASW | 80 | 0.066 |
| 100 | 2.9374 | 33.9216 | 27.0299 | 7.3299 | 24.067 | 2.517 | 7.143 | 27.2 | 9.7 | 3.2 | 13.8 | 2.5 | 0.74 | 3.7 | 0.58 | 4.6 | 1.4 | 5.0 | 0.73 | 5.0 | 0.92 | 0.23 | 0.01 | 0.32 | 0.002 | 1.24 | 0.06 | AASW | 100 | 0.059 |
| 130 | 2.1087 | 33.9355 | 27.1104 | 7.2748 | 26.252 | 2.582 | 16.250 | 22.9 | 7.2 | 2.9 | 13.2 | 2.3 | 0.76 | 3.6 | 0.56 | 4.5 | 1.3 | 4.8 | 0.69 | 4.7 | 0.86 | 0.20 | 0.01 | 0.27 | 0.002 | 1.33 | 0.07 | WW | 150 | 0.077 |
| 300 | 1.6498 | 34.1682 | 27.3317 | 5.8410 | | | | 23.7 | 5.3 | 2.9 | 13.0 | 2.3 | 0.71 | 3.5 | 0.57 | 4.6 | 1.4 | 5.0 | 0.76 | 5.2 | 0.94 | 0.14 | 0.01 | 0.27 | 0.001 | 1.26 | 0.06 | UCDW | 200 | 0.14 |
| 480 | 2.1715 | 34.3898 | 27.4692 | 4.4996 | 39.763 | 3.173 | 83.565 | 24.9 | 7.8 | 3.4 | 15.1 | 2.7 | 0.74 | 3.7 | 0.61 | 5.0 | 1.4 | 5.3 | 0.78 | 5.5 | 0.99 | 0.19 | 0.01 | 0.27 | 0.002 | 1.17 | 0.06 | UCDW | 300 | 0.17 |
| | | | | | | | | | | | | | | | | | | | | | | | | | | | | | 400 | 0.24 |
| | | | | | | | | | | | | | | | | | | | | | | | | | | | | | 450 | 0.25 |
| | | | | | | | | | | | | | | | | | | | | | | | | | | | | | 500 | 0.32 |

| | | | | | | | | | | | | | | | | | | | | | | | | | | | | | |
|---|---|---|---|---|---|---|---|---|---|---|---|---|---|---|---|---|---|---|---|---|---|---|---|---|---|---|---|---|---|
| A3 (50°42.32′S 71°59.83′E; water depth, 482 m; 4 January 2005) | | | | | | | | | | | | | | | | | | | | | | | | | | | | | |
| 0 | 3.6099 | 33.8980 | 26.9485 | 7.4039 | | | | 21.8 | 9.5 | 2.9 | 12.4 | 2.2 | 0.69 | 3.2 | 0.50 | 4.2 | 1.3 | 4.6 | 0.69 | 4.6 | 0.82 | 0.27 | 0.02 | 0.28 | 0.003 | 1.32 | 0.06 | AASW | | |
| 20 | 3.5914 | 33.8981 | 26.9503 | 7.4181 | 22.609 | 1.570 | 1.878 | 23.1 | 9.3 | 3.2 | 13.8 | 2.5 | 0.78 | 3.6 | 0.55 | 4.5 | 1.3 | 4.8 | 0.69 | 4.6 | 0.86 | 0.24 | 0.02 | 0.30 | 0.003 | 1.34 | 0.05 | AASW | 40 | 0.11 |
| 50 | 3.5865 | 33.8984 | 26.9510 | 7.3960 | | | | 21.1 | 8.0 | 2.9 | 13.1 | 2.3 | 0.69 | 3.5 | 0.57 | 4.4 | 1.3 | 4.8 | 0.71 | 4.9 | 0.85 | 0.23 | 0.01 | 0.25 | 0.002 | 1.22 | 0.06 | AASW | 80 | 0.12 |
| 100 | 3.4647 | 33.9009 | 26.9647 | 7.3374 | 24.958 | 2.098 | 4.508 | 22.8 | 9.9 | 3.1 | 13.8 | 2.4 | 0.77 | 3.6 | 0.59 | 4.5 | 1.3 | 5.0 | 0.71 | 4.9 | 0.91 | 0.26 | 0.01 | 0.26 | 0.003 | 1.30 | 0.06 | AASW | 150 | 0.11 |
| 150 | 1.5834 | 33.9559 | 27.1662 | 7.1833 | 29.362 | 2.691 | 18.594 | 22.7 | 8.0 | 3.0 | 13.2 | 2.4 | 0.78 | 3.5 | 0.55 | 4.7 | 1.3 | 5.0 | 0.70 | 5.0 | 0.91 | 0.22 | 0.01 | 0.27 | 0.002 | 1.35 | 0.06 | WW | 200 | 0.19 |
| 250 | 1.3728 | 34.0553 | 27.2608 | 6.5726 | | | | 22.2 | 6.8 | 2.9 | 13.4 | 2.2 | 0.71 | 3.5 | 0.56 | 4.4 | 1.3 | 4.8 | 0.67 | 5.1 | 0.91 | 0.19 | 0.01 | 0.26 | 0.002 | 1.28 | 0.05 | WW | 300 | 0.20 |
| 350 | 1.8653 | 34.2182 | 27.3557 | 5.5288 | | | | 23.6 | 6.5 | 3.1 | 13.4 | 2.4 | 0.79 | 3.7 | 0.57 | 4.7 | 1.3 | 5.1 | 0.75 | 5.1 | 0.95 | 0.17 | 0.01 | 0.25 | 0.002 | 1.34 | 0.06 | UCDW | 350 | 0.24 |
| 400 | 1.9904 | 34.2908 | 27.4042 | 5.1336 | 39.052 | 2.723 | 61.263 | 23.5 | 7.6 | 3.2 | 14.0 | 2.4 | 0.78 | 3.7 | 0.60 | 4.7 | 1.4 | 5.1 | 0.73 | 5.2 | 1.01 | 0.20 | 0.01 | 0.25 | 0.002 | 1.31 | 0.07 | UCDW | | |
| 450 | 2.1307 | 34.3617 | 27.4499 | 4.7132 | 40.520 | 2.855 | 73.056 | 25.3 | 8.7 | 3.5 | 14.4 | 2.5 | 0.77 | 3.9 | 0.61 | 4.8 | 1.4 | 5.2 | 0.78 | 5.3 | 1.03 | 0.21 | 0.01 | 0.27 | 0.002 | 1.26 | 0.06 | UCDW | | |
| A11 (49°09.14′S 74°00.01′E; water depth, 2527 m; 21 January 2005) | | | | | | | | | | | | | | | | | | | | | | | | | | | | | |
| 20 | 3.8225 | 33.9059 | 26.9338 | 7.2522 | 28.979 | 1.914 | 3.171 | 21.4 | 5.7 | 2.8 | 12.4 | 2.4 | 0.56 | 3.6 | 0.55 | 4.8 | 1.3 | 5.0 | 0.75 | 5.0 | 0.8 | 0.16 | 0.01 | 0.25 | 0.001 | 0.99 | 0.06 | AASW | 40 | 0.085 |
| 60 | 3.4403 | 33.9119 | 26.9758 | 7.3055 | 28.318 | 1.815 | 2.731 | 20.7 | 4.5 | 2.7 | 12.0 | 2.3 | 0.71 | 3.5 | 0.56 | 4.5 | 1.3 | 4.9 | 0.69 | 4.7 | 0.9 | 0.13 | 0.01 | 0.26 | 0.001 | 1.27 | 0.05 | AASW | 125 | 0.088 |
| 100 | 2.8993 | 33.9248 | 27.0358 | 7.2757 | 30.867 | 2.112 | 9.073 | 21.5 | 5.1 | 2.8 | 12.5 | 2.3 | 0.67 | 3.7 | 0.56 | 4.5 | 1.4 | 4.9 | 0.74 | 4.8 | 0.9 | 0.15 | 0.01 | 0.24 | 0.001 | 1.18 | 0.06 | WW | 200 | 0.082 |
| 200 | 1.4751 | 34.0677 | 27.2637 | 6.4024 | 42.666 | 2.607 | 46.070 | 36.9 | 5.1 | 5.3 | 23.3 | 4.2 | 1.17 | 6.2 | 0.95 | 7.4 | 2.0 | 7.1 | 1.05 | 7.6 | 1.3 | 0.08 | 0.005 | 0.27 | 0.001 | 1.17 | 0.04 | WW | 400 | 0.088 |
| 500 | 2.1017 | 34.4547 | 27.5268 | 4.4182 | | | | 28.8 | 4.3 | 3.8 | 16.9 | 2.9 | 0.80 | 4.7 | 0.71 | 5.9 | 1.7 | 6.1 | 0.91 | 6.5 | 1.1 | 0.09 | 0.01 | 0.25 | 0.001 | 1.12 | 0.06 | UCDW | 600 | 0.14 |
| 600 | 2.2301 | 34.6264 | 27.6539 | 4.0199 | 36.727 | 2.739 | 83.421 | 24.9 | 4.1 | 3.1 | 13.9 | 2.6 | 0.66 | 3.9 | 0.60 | 5.0 | 1.4 | 5.4 | 0.78 | 5.5 | 1.0 | 0.10 | 0.01 | 0.27 | 0.001 | 1.08 | 0.05 | UCDW | 1000 | 0.16 |
| 1500 | 1.8754 | 34.7443 | 27.7767 | 4.3863 | 33.698 | 2.508 | 88.634 | 24.7 | 4.3 | 3.0 | 13.5 | 2.4 | 0.66 | 3.8 | 0.56 | 5.1 | 1.4 | 5.5 | 0.77 | 5.9 | 1.0 | 0.11 | 0.01 | 0.24 | 0.001 | 1.14 | 0.06 | LCDW | 1500 | 0.17 |
| 2500 | 0.8015 | 34.7185 | 27.8321 | 4.6964 | 35.401 | 2.673 | 102.626 | 23.9 | 6.1 | 2.9 | 12.6 | 2.2 | 0.57 | 3.4 | 0.54 | 4.5 | 1.3 | 4.9 | 0.68 | 4.9 | 0.9 | 0.16 | 0.01 | 0.29 | 0.002 | 1.05 | 0.04 | LCDW | | |
| KERFIX (50°40.40′S 68°25.20′E; water depth, 1614 m; 10 February 2005)[b] | | | | | | | | | | | | | | | | | | | | | | | | | | | | | |
| 0 | 3.6959 | 33.8218 | 26.8794 | 7.3412 | 23.707 | 2.121 | 7.333 | 18.0 | 3.3 | 2.2 | 10.3 | 1.9 | 0.59 | 3.1 | 0.50 | 4.2 | 1.2 | 4.6 | 0.67 | 4.5 | 0.8 | 0.12 | 0.01 | 0.24 | 0.001 | 1.21 | 0.07 | AASW | 40 | 0.14 |
| 50 | 3.6968 | 33.8221 | 26.8795 | 7.3359 | 23.707 | 2.227 | 7.333 | 17.5 | 3.3 | 2.3 | 10.5 | 1.8 | 0.47 | 3.1 | 0.51 | 4.2 | 1.3 | 4.6 | 0.68 | 4.6 | 0.8 | 0.12 | 0.01 | 0.20 | 0.001 | 0.99 | 0.04 | AASW | 80 | 0.089 |
| 100 | 3.4297 | 33.8287 | 26.9105 | 7.3110 | 23.835 | 2.333 | 7.333 | 16.9 | 3.4 | 2.3 | 10.6 | 1.8 | 0.48 | 3.0 | 0.51 | 4.3 | 1.3 | 4.6 | 0.68 | 4.6 | 0.8 | 0.12 | 0.01 | 0.19 | 0.001 | 1.01 | 0.04 | AASW | 120 | 0.075 |
| 200 | 1.5239 | 33.9615 | 27.1750 | 7.1008 | 29.826 | 2.793 | 25.153 | 20.6 | 5.7 | 2.8 | 12.1 | 2.1 | 0.54 | 3.3 | 0.53 | 4.5 | 1.3 | 4.8 | 0.71 | 5.0 | 0.9 | 0.17 | 0.01 | 0.25 | 0.001 | 1.03 | 0.03 | WW | 150 | 0.12 |
| 500 | 2.2956 | 34.3738 | 27.4463 | 4.5114 | 36.071 | 3.252 | 68.049 | 20.1 | 4.5 | 2.7 | 12.2 | 2.1 | 0.59 | 3.4 | 0.56 | 4.6 | 1.4 | 5.0 | 0.75 | 5.3 | 1.0 | 0.14 | 0.01 | 0.21 | 0.001 | 1.09 | 0.04 | UCDW | 300 | 0.16 |
| 600 | 2.2472 | 34.5836 | 27.6181 | 4.1281 | 33.904 | 3.182 | 80.032 | 33.5 | 27.5 | 5.7 | 23.7 | 4.2 | 1.06 | 5.1 | 0.83 | 6.2 | 1.7 | 6.0 | 0.90 | 6.2 | 1.1 | 0.46 | 0.05 | 0.32 | 0.009 | 1.13 | 0.06 | UCDW | 400 | 0.21 |
| 1200 | 2.0856 | 34.7234 | 27.7432 | 4.3285 | 31.100 | 3.075 | 86.156 | 31.4 | 15.7 | 4.7 | 19.8 | 3.4 | 0.90 | 4.8 | 0.74 | 5.9 | 1.6 | 5.8 | 0.93 | 6.2 | 1.1 | 0.29 | 0.02 | 0.30 | 0.004 | 1.15 | 0.08 | UCDW | 500 | 0.25 |
| 1550 | 1.6973 | 34.7594 | 27.8025 | 4.6344 | 29.826 | 3.040 | 94.526 | 30.2 | 8.9 | 4.5 | 19.7 | 3.5 | 0.89 | 4.9 | 0.78 | 6.3 | 1.8 | 6.1 | 0.93 | 6.5 | 1.2 | 0.17 | 0.01 | 0.24 | 0.001 | 1.08 | 0.02 | LCDW | 1000 | 0.36 |
| | | | | | | | | | | | | | | | | | | | | | | | | | | | | | 1500 | 0.31 |
| PAAS[c] | | | | | | | | 275.0 | 568.0 | 62.7 | 235.0 | 36.9 | 7.1 | 29.6 | 4.9 | 28.8 | 6.0 | 17.0 | 2.4 | 16.3 | 2.5 | | | | | | | | | |

[a]Data from Blain et al. (2008).

[b]The seawater samples at these stations are filtered with Versapore 0.8 μm pore size filters; the other samples are filtered with Durapore 0.65 μm pore size filters.

[c]Average of Post-Archean Australian Sedimentary Shales (PAAS) (Taylor and McLennan, 1985) values are given in $\mu mol\,kg^{-1}$.

## 4. Results

### 4.1. REE concentrations

Dissolved REE concentrations are reported in Table 1 along with dissolved Fe concentrations (Blain et al., 2008) and hydrographic data. The REE vertical profiles for stations KERFIX, C1, C11, B11, A3, A11 are plotted in Fig. 2A, together with AJAX cruise data (Atlantic sector of the Southern Ocean, cf. Fig. 1 German et al., 1995). Except for Ce, the REE profiles are characterized by relatively low concentrations in the upper part of the water column, increasing progressively with depth, consistent with the classical REE oceanic behaviour (Elderfield and Greaves, 1982; De Baar et al., 1983, 1985).

The vertical Ce profiles display a shape that is different from those of the other REE, reflecting its particular behaviour (Sholkovitz and Schneider, 1991; Sholkovitz et al., 1992; Moffett, 1994). Surface waters are characterized by relatively high Ce concentrations, remaining nearly constant at depth.

At the open-ocean station KERFIX, average REE concentrations are about 25% higher than those measured in the Atlantic sector of the Southern Ocean and in the Madagascar basin (Bertram and Elderfield, 1993; German et al., 1995). Except at 800 m, feature discussed later, KERFIX profile shapes and values are consistent with the location of this station, farther downstream within the global thermohaline circulation than stations documented by these authors. Note that, when considering the full depth profiles, C11 and B11 (east of the plateau) and C5 (south transect of the plateau) display REE concentrations similar to those observed at KERFIX. Focusing now on the layer shallower than 500 m depth, which roughly corresponds to the plateau depth, almost all the REE concentrations are found larger than or equal to those measured at KERFIX, as shown in Fig. 2B. The highest values are found at station C1 (likely reflecting the close proximity of this shallow station to the Heard Island; see Fig. 1). These enrichments, relative to KERFIX are quantified as follows:

$$[\mathrm{REE}]_{xs} = [\mathrm{REE}]_{m} - [\mathrm{REE}]_{Ker}, \quad (1)$$

where the subscripts xs, m and Ker refer to REE concentrations in excess, measured in the water mass above the plateau and within the same water mass at KERFIX, respectively. Ranges of these relative enrichments (depth < 500 m) are 15–90% for La, 10–80% for Nd and 8–20% for Yb. As already underlined, these enrichments are not significant at C5, and in the deep waters (below 500 m) of C11 and B11.

In addition to the generally higher concentrations over the plateau, significant concentration maxima were found around 800 m depth at station KERFIX and at ~200 m depth at station A11. The origins of these features are discussed in Section 5.4.

### 4.2. REE patterns

REE patterns are obtained by normalizing the sample to the Post-Archean Australian Sedimentary rocks REE contents (Taylor and McLennan, 1985). Two contrasted REE patterns are displayed in Fig. 3A. The KERFIX 100-m pattern displays the general shape of open-ocean seawaters, i.e. pronounced Ce anomaly and a clear HREE/LREE enrichment, whereas the C1 100-m pattern reveals recent lithogenic contribution identified by an attenuated Ce anomaly and a flatter pattern. The Ce anomaly is quantified as follows:

$$\mathrm{Ce/Ce*} = 2[\mathrm{Ce}]_n/([\mathrm{La}]_n + [Pr]_n), \quad (2)$$

where $[\mathrm{Ce}]_n$, $[\mathrm{La}]_n$ and $[\mathrm{Pr}]_n$ are the shale normalized concentrations. Heavy versus light REE enrichment is quantified by $(\mathrm{La/Yb})_n = [\mathrm{La}]_n/[\mathrm{Yb}]_n$. Values close to 0 correspond to pronounced Ce anomalies and HREE/LREE enrichments, whereas values close to 1 correspond to slight Ce anomalies and HREE/LREE enrichments. Ce anomaly and $(\mathrm{La/Yb})_n$ values are reported in Table 1 and displayed in Fig. 4A.

The REE patterns of nearly all of the samples display a slight positive Gd anomaly, and a variable Eu anomaly, quantified as follows.

$$\mathrm{Eu/Eu*} = 3[\mathrm{Eu}]_n/(2[\mathrm{Sm}]_n + [\mathrm{Tb}]_n), \quad (3)$$

where $[\mathrm{Eu}]_n$, $[\mathrm{Sm}]_n$ and $[\mathrm{Tb}]_n$ are the shale normalized concentrations of these elements. Terbium is used here as a reference instead of Gd, commonly used. Indeed, since most of the seawater samples show a slight Gd anomaly, the use of Gd as a reference would have negatively biased the estimation of Eu* in these samples.

The origin of this seawater Gd enrichment is not clear yet, although it has been already observed by many authors (Alibo and Nozaki, 1999). Because ICP/MS measurements of Eu and Gd are specifically subject to oxy–hydroxides interferences, one could suspect analytical artefact. However, interferences are thoroughly corrected in our protocol and special care was taken in the validation of these data, by monitoring the interference levels and the consistencies of the two Eu and 3 Gd isotope measurements. Using Tb as reference for the Eu* calculation for the basalts as well as for the seawater makes the comparison between both material clearer.

## 5. Discussion

### 5.1. Dissolved REE enrichments over the plateau

According to Eq. (1), subtracting the average REE concentration at Kerfix (< 500 m) from the average REE concentration over the plateau yields the average upper-layer REE excess of the plateau. Resulting average enrichments are $[\mathrm{Nd}]_{xs} = 2.8 \pm 0.5(1\sigma_n)\,\mathrm{pmol\,kg^{-1}}$ and $[\mathrm{Yb}]_{xs} = 0.3 \pm 0.16(1\sigma_n)\,\mathrm{pmol\,kg^{-1}}$. These high REE contents suggest that terrigenous inputs are influencing the

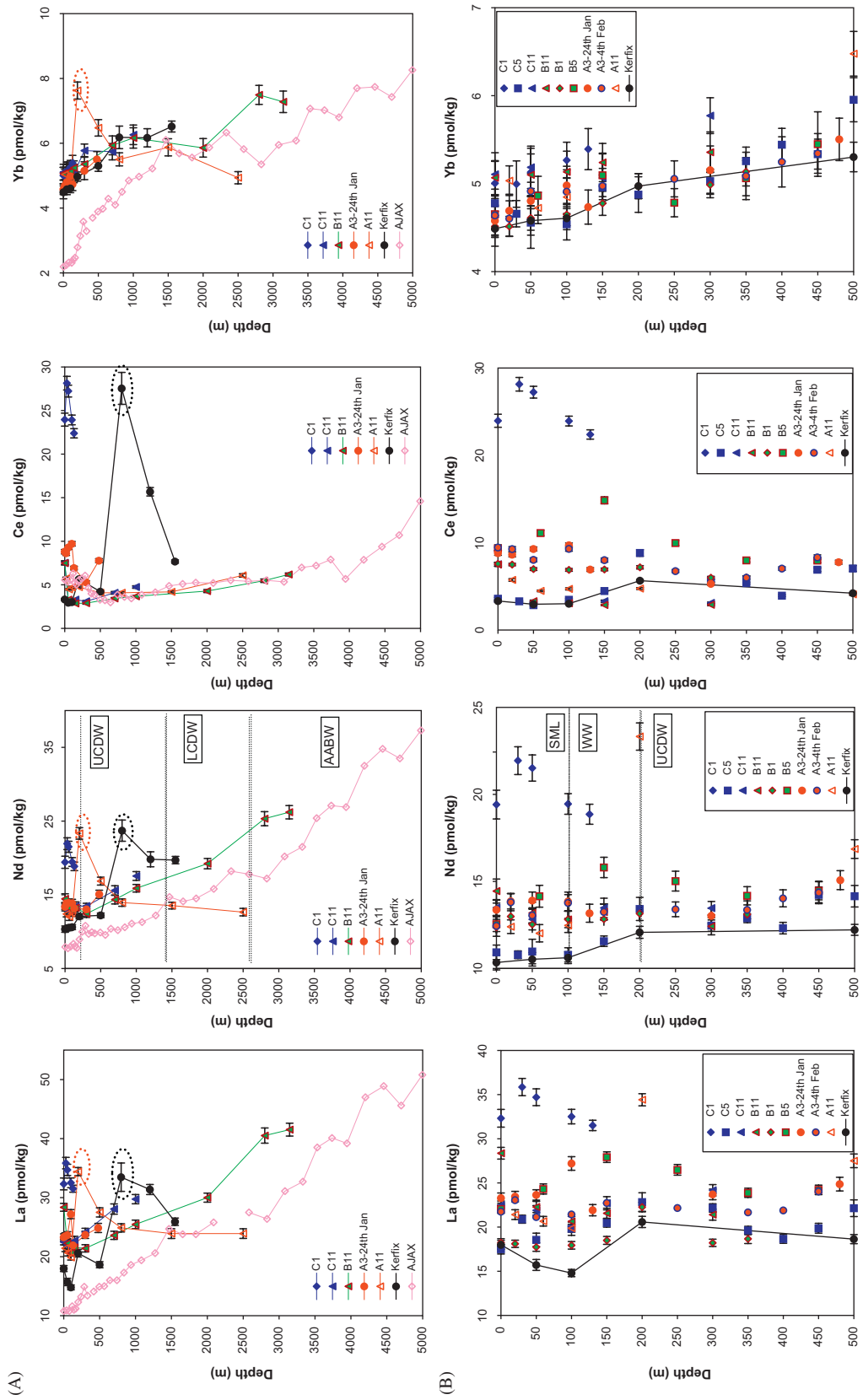


Fig. 2. Upper panel (A): Vertical profiles of dissolved REE at stations Kerfix, C1,C11, B11, A3, A11 compared to those of AJAX (Bertram and Elderfield, 1993). Lower panel (B): The detailed REE concentrations for the upper 500 m were also plotted for all the stations of this study. Water masses are identified on the Nd profiles (SML: surface mixed layer; UCDW: upper circumpolar deep water; LCDW: lower circumpolar deep water; AABW: Antarctic bottom water).

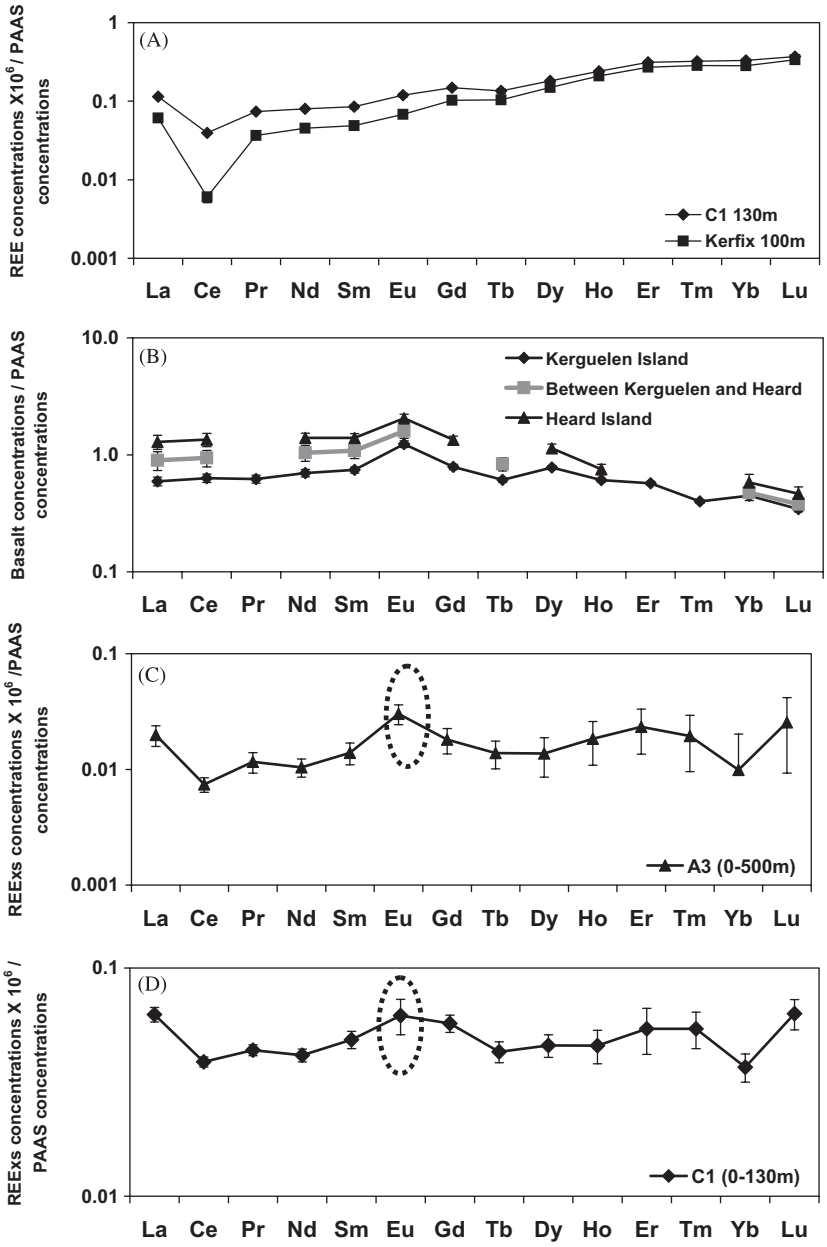


Fig. 3. "PAAS" normalized REE patterns: (A) REE patterns in the seawater at station C1 (100 m) and Kerfix (100 m); (B) REE patterns of the Kerguelen archipelago basalts (Barling et al., 1994; Weis et al., 2002; Doucet et al., 2005); (C) REE patterns of the enrichment at station C1 averaged on the entire water column and (D) REE patterns of the enrichment at station A3 averaged on the entire water column.

chemistry of the plateau surface waters. This assumption, the source and magnitude of this potential external input are discussed below.

Cerium anomalies (Fig. 4A) are relatively high at stations C1, B1, B5 and A3, whereas $(La/Yb)_n$ values are relatively high at stations C1, B5 and A3, with intermediate values at C11, B11 and A11. These high values reflect recent dissolution of lithogenic material. The much higher values measured at C1 likely reflect more recent lithogenic inputs, likely due to the close vicinity of the Heard Island. On the whole, despite some differences in the spatial distribution of these two parameters, these data confirm the occurrence of recent dissolution of terrigeneous material over the plateau, in contrast to station KERFIX.

Flood basalts are the dominant volcanic products on the Kerguelen archipelago, covering 85% of its surface (Doucet et al., 2005). PAAS-normalized REE patterns of these basalts, displayed in Fig. 3B, show an Eu anomaly of ~1.6 (Weis et al., 2002), which can be considered as a signature of this lithogenic source.

Since Eu is known to behave like the other trivalent REE in the ocean, positive Eu anomalies are usually not observed in seawater (Kato et al., 1998; Tachikawa et al.,

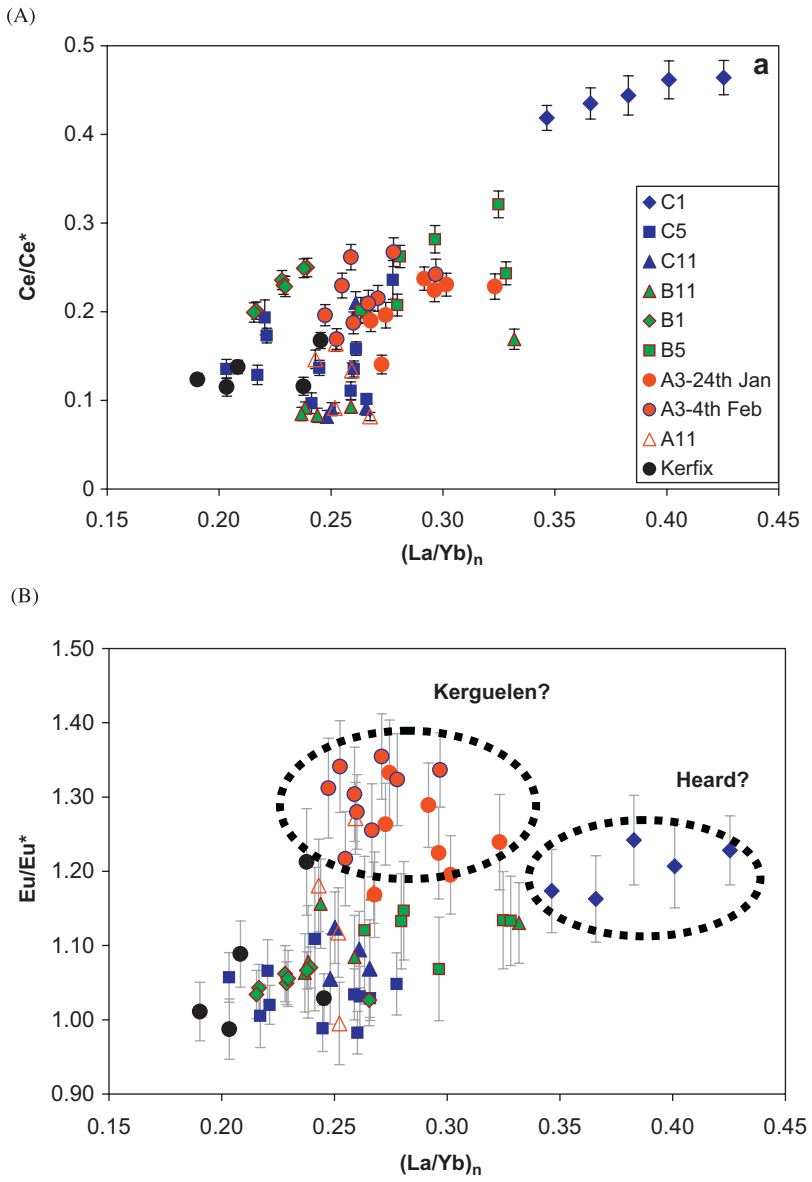


Fig. 4. (A) Ce anomaly versus $(La/Yb)_n$ in the upper layer (<500 m) for all the stations and (B) Eu anomaly versus $(La/Yb)_n$ in the upper layer (<500 m) for all the stations.

1999). The KEOPS area stands in contrast with this general feature, significant positive Eu anomalies ($Eu/Eu^* > 1.15$) being observed at stations C1 and A3 throughout the water column, in AASW and WW at A11, in WW at B11 and in the surface sample of KERFIX (see Table 1, Fig. 4B). On the other hand, several samples (e.g., stations B1 and C5) do not display any significant Eu anomaly.

In order to characterize the potential external source, the REE patterns of the enrichments (calculated by subtracting KERFIX from plateau data, according to Eq. (1)) are displayed in Fig. 3C and D for two stations, A3 and C1. Eu anomalies of these enrichments are observed for the whole water column of station A3 ($2.2 \pm 0.44$) and C1 ($1.4 \pm 0.07$), in the WW and the UCDW (bottom sample) at B5, and in the WW at A11 and B11. Again, the occurrence of significant Eu anomalies in the seawater samples and in the calculated enrichments suggests that the high REE contents observed in the filtered waters of the plateau results from the dissolution of the lithogenic material from Kerguelen and/or Heard islands.

More surprising is the Eu anomaly observed at the surface at station Kerfix. Neither the dominant surface current (eastwards, Fig. 1) nor the dominant wind directions at this site (Jeandel et al., 1998a) help constrain the source of this enrichment. Since the extreme surface only is affected (the two other AASW samples at KERFIX are not), our favourite candidate would be a sporadic aeolian input event, carrying dust from the Kerguelen Island. Actually, such event did occur the day before sampling: the wind (daily mean of $\sim 40\,km\,h^{-1}$) blew southwestwards from the Kerguelen Island towards KERFIX (on board data not shown).

Other tracers led to suspect a significant, although heterogeneous, lithogenic influence over the Kerguelen Plateau, together with occurrence of horizontal transports: $^{228}Ra/^{226}Ra$, (van Beek et al., 2008), $^{232}Th$ (Venchiarutti et al., 2008) and lithogenic suspended Ba (Jacquet et al., 2008). Although the lithogenic influence on the plateau-water trace element content is clear and revealed by different tracers, it is also heterogeneously distributed: some stations like C1, A3, B5, A11 are affected, whereas others are not. Such heterogeneity likely reflects the complex circulation scheme, but the resolution of the plateau dynamic description prevents us to interpret the present set of data further (Park et al., 2008b). In addition, scavenging processes (e.g., oxidation and adsorption), which likely occur in this particle-rich environment, may weaken the Eu anomalies and slightly affect the REE patterns. Further Nd isotope and suspended particle analyses will help to better constrain dissolved/particulate processes.

### 5.2. Sources and fluxes of REE and Fe from Kerguelen Plateau

Two possible external sources could provide lithogenic material to the plateau waters: the Kerguelen and Heard islands, respectively, located in the northwest and southwest of the plateau. Both belong to the same geological unit, mainly flood basalts with similar geochemical characteristics, more particularly their REE patterns and Eu anomalies (Doucet et al., 2005). However, the Eu anomalies at station A3 are slightly higher than those measured at station C1, whereas Ce/Ce* and $(La/Yb)_n$ values at station A3 are significantly lower than at station C1 (Fig. 4A). These differences could argue for two different external sources: the Kerguelen Island could provide material to the northernmost KEOPS stations, whereas the Heard Island could provide material to the other stations. Although published basalt Eu* anomalies do not clearly discriminate between both origins (Weis et al., 2002), high Eu* anomalies in some Kerguelen island fields could occur (D. Weis, personal communication).

Although the main current direction over the Kerguelen Plateau is northwestwards and the KEOPS sampling area seems to be isolated from any Kerguelen influence by the strong jet contouring the Kerguelen Island by the south (Fig. 1; Blain et al., 2008; Mongin et al., 2008), one cannot exclude that the northernmost stations received waters enriched in dissolved lithogenic elements, coming from the Kerguelen shelf, due to sporadic mesoscale intrusions from north of the PF (Rosemary Morrow, personal communication). This is also supported by the occurrence of eddy activities observed by Mongin et al. (2008). A second possibility for Kerguelen material to reach A3 (or its vicinity) could be bottom transport of shelf deposits (e.g., turbidites, contourities, etc.). The first mechanism would explain surface and subsurface enrichments without requiring an additional physical vector. The second requires enhanced vertical transport to spread the lithogenic contributions from the sediments up to the surface. Such vertical processes are supported by the occurrence of internal waves and significant vertical eddy diffusivities observed over the plateau (Park et al., 2008a). On the other hand, the lack of $^{228}Ra$ bottom enrichment at A3 has led Van Beek et al. (2008) to conclude that such vertical transport does not explain the $^{228}Ra$ enrichment observed at the subsurface of the same station. These authors favour the horizontal advection of shallow waters that were in recent contact with a shelf to explain the observed subsurface maxima. Similarly, Venchiarutti et al. (2008) observed $^{232}Th$ maxima in the subsurface waters of several plateau stations (including A3) that cannot be directly related to bottom $^{232}Th$ enrichment. These two studies argue against the bottom transport of shelf deposits from Kerguelen as an REE source for the upper layer of station A3. Furthermore, the high dissolved $^{228}Ra$ and $^{232}Th$ concentrations measured at station C1, together with the main current direction, lead van Beek et al. (2008) and Venchiarutti et al. (2008) to suggest a northwestward advection over the Kerguelen Plateau of waters that have interacted with the shallow sediments of the Heard Island shelf.

To sum up, REE pattern differences between A3 and C1 could argue in favour of a Kerguelen Island influence at A3, through sporadic mesoscale intrusion of waters through the PF. On the other hand, the main current direction over the Kerguelen Plateau (northwestwards, Fig. 1; Charrassin et al., 2004; Mongin et al., 2008; Park et al., 2008b) favours the Heard Island as the main source of dissolved lithogenic material in the plateau waters.

Once again, the complex circulation scheme characterizing the water transport on the plateau together with the scarcity of our dataset prevents any detailed identification of the exact trajectory of these inputs (Park et al., 2008b). Therefore, a simple one-box model is used to estimate the input of Nd, provided by this "external source", and required to account for the larger concentrations found in the waters overlying the plateau (Fig. 5). The water flux, $F_w$, is estimated by multiplying the section of the box (500 m depth and 350 km width, cf. Fig. 5) by the mean current velocity. The latter, measured between 3 and 5 cm $s^{-1}$ above the plateau (Park et al., 2008b), is estimated at $4 \pm 0.5(1\sigma)$ cm $s^{-1}$, yielding a water flux ($F_w$) of $\sim 7 \pm 1.0(1\sigma)$ Sv (taking into account 5% uncertainties, $1\sigma$, on the box dimensions; $1\sigma$ corresponding to a 68%

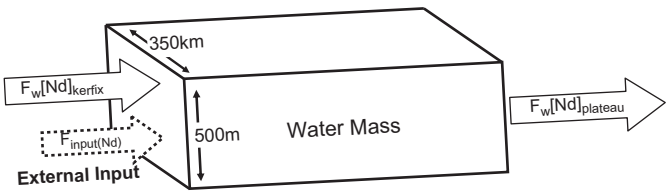


Fig. 5. Box model used to estimate the lithogenic dissolved Nd flux into the water above the Kerguelen Plateau.

confidence interval). Steady-state hypothesis and mass conservation imply that the input of external Nd is

$$F_{\text{input(Nd)}} = F_{\text{w}} \times ([\text{Nd}]_{\text{plateau}} - [\text{Nd}]_{\text{Kerfix}}), \quad (4)$$

where $[\text{Nd}]_{\text{Kerfix}} = 11.2 \pm 0.4 (1\sigma_n)$ pmol kg$^{-1}$ and $[\text{Nd}]_{\text{plateau}} = 14.0 \pm 0.3 (1\sigma_n)$ pmol kg$^{-1}$. These values represent the average concentrations measured between the surface and 500 m, at KERFIX and at all the plateau stations, respectively. The resulting Nd flux is $89 \pm 20 (1\sigma)$ t (Nd) y$^{-1}$. This value is likely underestimated since the occurrence of significant Ce anomalies in the plateau waters indicate that REE scavenging probably already occurred, likely lowering the REE contents of the plateau waters (Fig. 3; Sholkovitz et al., 1994; Tachikawa et al., 1999).

Since both iron and Nd are lithogenic, it is tempting to estimate the amount of iron that would be liberated from the same lithogenic source as Nd, mostly if direct basalt dissolution is involved. In most cases, abiotic solubilities of lithogenic materials have been estimated in the range 1–10% for Fe (Bonnet and Guieu, 2004; Boyle et al., 2005; Buck et al., 2006) and 2–10% for Nd (Jeandel et al., 1995; Tachikawa et al., 1999). Although Bonnet and Guieu (2004) also found Fe solubilities as low as 0.05% for Saharan dust in seawater, Oelkers and Gislason (2001) emphasized that basaltic glass dissolution reaches stoichiometric dissolution within several hours at neutral conditions. REE and Fe contained in these basalts are expected to follow this stoichiometric dissolution, allowing us to consider that they have close abiotic solubilities. In addition, Haley et al. (2004) suggest that the release of REE from the sediments is due to the dissolution of Fe phases. Therefore, we assume that Fe and Nd dissolve concomitantly and in the same proportion, within 50% uncertainty ($2\sigma$, 95% confidence interval). Using the Fe/Nd ratios in the Kerguelen basalts ($3370$ g g$^{-1} \pm 20\%$, $2\sigma$, Doucet et al., 2005) yield an Fe flux of 300,000 t(Fe) y$^{-1} \pm 200{,}000$ ($2\sigma$, 95% confidence interval; overall uncertainty calculated by propagating the uncertainties of all the variables described above, cf. Table 2). This leads a lower limit of 100,000 t(Fe) y$^{-1}$ for the external Fe input. Since this result is based on a likely underestimated Nd flux (as described above), it is also likely underestimated. Overall, this result should be considered cautiously, keeping in mind the steady-state assumption.

Table 2
Terms used for the Nd and Fe budget calculations, with their uncertainties, expressed as $1\sigma$ (68% confidence level)

| | |
|---|---|
| Mean Nd concentration at Kerfix (pmol kg$^{-1}$, depth < 500m)[a] | $11.2 \pm 0.4$ |
| Mean Nd concentration over the plateau (pmol kg$^{-1}$)[b] | $14.0 \pm 0.3$ |
| Depth of the water mass (m) | $500 \pm 25$ |
| Width of the water mass (m) | $350{,}000 \pm 17{,}500$ |
| Current velocity (cm s$^{-1}$)[c] | $4 \pm 0.5$ |
| Fe/Nd ratio in the basalt (g g$^{-1}$)[d] | $3370 \pm 337$ |
| Fe/Nd solubility ratio (g g$^{-1}$)[e] | $1 \pm 0.25$ |
| Mean Fe concentration at Kerfix (pmol kg$^{-1}$, depth < 500m)[f] | $0.15 \pm 0.024$ |
| Mean Fe concentration over the plateau (pmol kg$^{-1}$)[g] | $0.20 \pm 0.029$ |
| Water flux ($10^8$ m$^3$ s$^{-1}$) | $7 \pm 1.0$ |
| Nd external input (t y$^{-1}$) | $89 \pm 20$ |
| Fe external input (t y$^{-1}$) | $300{,}000 \pm 100{,}000$ |

[a]Standard error, $n = 5$ for Kerfix.
[b]Standard error, $n = 60$, for all the stations on the plateau.
[c]From Park et al. (2008a, b).
[d]From Doucet et al. (2005).
[e]Bonnet and Guieu, (2004), Boyle et al. (2005), Buck et al. (2006), Jeandel et al. (1995), Tachikawa et al. (1999), Oelkers and Gislason (2001).
[f]Standard error, $n = 7$ for Kerfix.
[g]Standard error, $n = 52$, for all the stations on the plateau.

### 5.3. Different behaviours for REE and Fe on the plateau

Despite these estimations of very significant dissolved Nd and Fe contributions, dissolved Fe is strongly depleted in the upper layers of the plateau, in contrast to REE (Blain et al., 2008). This observation clearly prevents the direct use of Nd (and REE) as proxy for Fe in seawater. Dissolved Fe depletion occurs very close to Heard, since at C1 the dissolved Fe/Nd ratio is of 15.3 g g$^{-1}$, far below the basalt ratios ($3370 \pm 337 (1\sigma)$ g g$^{-1}$). This discrepancy could reflect different dissolution rates between both elements, although never observed so far and which would be surprising if the whole basalt rocks are dissolved, and/or more likely, different behaviours of the two elements regarding the removal processes.

Can the biological assimilation of Fe explain the difference? Phytoplankton uptake estimated from $^{55}$Fe experiments during the cruise was about $208 \pm 77$ nmol Fe m$^{-2}$ d$^{-1}$ over an area of 45,000 km$^2$, which corresponds to $190 \pm 70$ t (Fe) y$^{-1}$ (Blain et al., 2007), at least three orders of magnitude smaller than the estimated lithogenic dissolved-Fe addition. Unless in vitro experiments greatly underestimate the phytoplankton assimilation rates, or admitting an unlikely $10^3$-fold increase of the biological activity at the contact of Heard (not revealed by the satellite images, Mongin et al., 2008), this active biological process alone cannot account for the observed dissolved iron "loss".

Another possibility would be that Fe is transferred from the dissolved phase to other phases. These could include large particles (via oxidation or adsorption processes) that would be removed towards the sediment, or complexes, colloids or small particles that would remain within the water masses (DFe concentrations reported by Blain et al., 2008, do not include these Fe fractions). This last hypothesis (suspended particles, complexes or colloids) is more likely, since total dissolvable Fe concentrations (TDFe, measurements made after 18 months at pH = 2; unpublished data, F. Chever, personal comments) showed significantly higher values than dissolved Fe concentrations. This suggests that although the external lithogenic source is the same for Fe and REE, once in seawater, Fe speciation yields a distribution of the different Fe species, leaving only a small fraction of DFe; finally, the largest Fe pool is probably under colloidal or complexed forms.

These last processes are not thought to affect significantly the measurements of REE concentrations reported here, which could explain, at least partially, the Fe/REE cycle decoupling in seawater. Since the Fe bio-availability of these non-dissolved phases remains unclear, it is difficult to conclude on the biological impact of this suspected very important input of lithogenic iron. Nevertheless, despite a likely significant addition of dissolved lithogenic iron on the plateau waters, it appears that dissolved iron is depleted to rate-limiting levels (Blain et al., 2007). This stresses the fact that strong Fe fertilization does not imply non-limited waters.

Another constraint on these input/output fluxes onto the Kerguelen Plateau waters would be to estimate the tracer output fluxes by measuring their sedimentation rates. This is an ongoing work.

### 5.4. Specific features at 800 m depth at station KERFIX and in the WW of station A11

The dissolved REE concentration profile at KERFIX display a pronounced LREE (eg., La, Ce and Nd) maxima at 800 m depth (Fig. 2A). These data are supported by the underlying sample (1200 m depth), ruling out the hypothesis of a contamination. The very small Ce anomaly and flat REE patterns suggest that dissolution of lithogenic material could have occurred recently at these depths. A possible mechanism generating such input could be lateral transport of a nepheloid cloud. Indeed, submarine storms, yielding contourites and turbidites, could generate nepheloid layers off the steep shelf of the plateau. The likelihood of this hypothesis can be tested in the case of Nd. Concentration of this element at 800 m ($23\,pmol\,kg^{-1}$) is about $10\,pmol\,kg^{-1}$ greater than what would be expected from a regular increase with depth. The Nd concentration in the Kerguelen basalts is about $26\times10^{-6}\,g\,g^{-1}$ (Doucet et al., 2005). Assuming that the nepheloids are composed of this basalt only—not completely realistic in the relatively productive KERFIX area—this hypothesis will yield a lower value if 2–10% of the Nd present on these particles dissolves, particle concentrations of $550–2750\,\mu g\,l^{-1}$ would be required to account for the observed increase. Although these values are lower limits, they are realistic, suggesting that the dissolution of particles could explain the observed maximum at 800 m depth at KERFIX. This is, however, a rough estimate. Further data such as the particulate REE concentrations and Nd isotope compositions could help to better understand the precise processes occurring in this water layer.

REE (except Ce) concentration maxima are observed in the WW (200 m) of station A11. The salinity in this layer (~34.1) is significantly higher than the salinity of the WW at the other stations (less than 34.0), whereas its temperature is higher. It is therefore likely that the WW at station A11 are of different origin than those of the other stations, consistent with the observations of Park et al. (2008b). The pronounced REE fractionation observed in this layer, suggests that scavenging already affected the distribution of these elements in this water mass. Although Byrne and Kim (1990) have shown that biogenic silica is among the most efficient substrate to induce strong HREE/LREE fractionation during scavenging, the mechanism responsible of the observed pattern remains unclear.

## 6. Conclusions

Dissolved REE concentrations were determined at nine vertical profiles upstream from and over the Kerguelen Plateau. High REE concentrations relative to station KERFIX (taken as the "open-ocean" reference) characterize the upper layers (<500 m) at most of the plateau stations. Relatively slight Ce anomalies and HREE/LREE enrichments suggest the occurrence of recent dissolution of lithogenic material. The positive Eu anomaly characterizing the Kerguelen archipelago basalts and observed in these enriched waters suggests that this material is weathered from the Kerguelen and/or Heard islands. On the one hand, different REE patterns in the southern and northern parts of the plateau, could suggest that Kerguelen Island material reaches the northernmost KEOPS stations within mesoscale structures. On the other hand, the general circulation scheme, in agreement with radium isotope distribution together with significant lithogenic enrichments evidenced in the vicinity of the Heard Island, suggests that this island is the main source of lithogenic material for the plateau waters.

A simple one-box model was used to quantify a lower limit for the dissolved Nd external input at $89\pm20\,t\,(Nd)\,y^{-1}$ and a simultaneous dissolved iron flux larger than $100{,}000\,t\,(Fe)\,y^{-1}$. The significant dissolved Nd and Fe addition contrast with the strong Fe depletion in the upper layers of the plateau, preventing the direct use of Nd (and REE) as a DFe proxy within the ocean (Nd was only used here to estimate dissolved Fe input into the plateau waters). Phytoplankton uptake alone cannot account for this discrepancy. The "missing iron" could probably be found in the colloidal and other iron phases, which are identified when measuring TDFe, underlining the different speciations characterizing iron and REE in seawater. Although significant dissolution of lithogenic material is likely fueling the waters flowing above the Kerguelen Plateau, almost all of its iron quickly disappears from the dissolved phase to either a colloid phase or the solid phase, yielding an iron limitation in the fertilized waters. Our results show that dissolved REE in such a coastal environment could help to understand better the dissolved Fe supply and consequently removal processes. However, better documentation on processes yielding Fe and REE decoupling is needed. Nd isotopic compositions, Fe and REE concentrations in the particle pool and the sediments are underway, which will likely help to investigate more precisely these processes.

## Acknowledgements

We thank two anonymous reviewers for their fruitful comments. This work was supported by the IPEV (Institute Paul—Emile Victor) and the INSU/CNRS (LEFE/ CYBER program), the LEGOS (CNRS, Toulouse, France). We are grateful to Stéphane Blain (KEOPS PI), for his scientific management of the project. We thank Marc Souhaut and Pieter van Beek for carrying out the sampling and Frederic Candaudap (ICP-MS) for the technical assistance. We appreciate helpful comments from Tom Trull and Geraldine Sarthou.

## References

Alibo, D.S., Nozaki, Y., 1999. Rare earth elements in Seawater: particle association, Shale-normalization and Ce oxidation. Geochimica et Cosmochimica Acta 63, 363–372.

Arsouze, T., Dutay, J.-C., Lacan, F., Jeandel, C., 2007. Modeling the neodymium isotopic composition with a global ocean circulation model. Chemical Geology 239 (1–2), 165–177.

Barling, J., Goldstein, S.L., Nicholis, I.A., 1994. Geochemistry of Heard Island (Southern Indian Ocean): characterization of an enriched mantle component and implications for enrichment of Sub-Indian Ocean Mantle. Journal of Petrology 35 (4), 1017–1053.

Barroux, G., Sonke, J.E., Boaventura, G., Viers, J., Godderis, Y., Bonnet, M.P., Sondag, F., Gardoll, S., Lagane, C., Seyler, P., 2006. Seasonal dissolved rare earth element dynamics of the Amazon River main stem, its tributaries, and the Curuai floodplain. Geochemistry, Geophysics, Geosystems 7.

Bertram, C.J., Elderfield, H., 1993. The geochemical balance of the rare earth elements and Nd isotopes in the oceans. Geochimica et Cosmochimica Acta 57, 1957–1986.

Blain, S., Treguer, P., Belviso, S., Bucciarelli, E., Denis, M., Desabre, S., Fiala, M., Jezequel, V.M., Le Fevre, J., Mayzaud, P., Marty, J.C., Razouls, S., 2001. A biogeochemical study of the island mass effect in the context of the iron hypothesis: Kerguelen Islands, Southern Ocean. Deep-Sea Research I 48 (1), 163–187.

Blain, S., Queguiner, B., Armand, L., Belviso, S., Bombled, B., Bopp, L., Bowie, A., Brunet, C., Brussaard, C., Carlotti, F., Christaki, U., Corbiere, A., Durand, I., Ebersbach, F., Fuda, J.L., Garcia, N., Gerringa, L., Griffiths, B., Guigue, C., Guillerm, C., Jacquet, S., Jeandel, C., Laan, P., Lefevre, D., Lo Monaco, C., Malits, A., Mosseri, J., Obernosterer, I., Park, Y.H., Picheral, M., Pondaven, P., Remenyi, T., Sandroni, V., Sarthou, G., Savoye, N., Scouarnec, L., Souhaut, M., Thuiller, D., Timmermans, K., Trull, T., Uitz, J., van Beek, P., Veldhuis, M., Vincent, D., Viollier, E., Vong, L., Wagener, T., 2007. Effect of natural iron fertilization on carbon sequestration in the Southern Ocean. Nature 446 (7139).

Blain, S., Sarthou, G., Laan, P., 2008. Distribution of dissolved iron during the natural iron fertilisation experiment KEOPS (Kerguelen Plateau, Southern Ocean). Deep-Sea Research II, this issue [doi:10.1016/j.dsr2.2007.12.028].

Bonnet, S., Guieu, C., 2004. Dissolution of atmospheric iron in seawater. Geophysical Research Letters 31 (3), L03303.

Boye, M., van den Berg, C.M.G., De Jong, J.T.M., Leach, H., Croot, P.L., De Baar, H.J.W., 2001. Organic complexation of iron in the Southern Ocean. Deep-Sea Research I 48, 1477–1497.

Boyle, E.A., Bergquist, B.A., Kayser, R.A., Mahowald, N., 2005. Iron, manganese, and lead at Hawaii Ocean time-series station ALOHA: temporal variability and an intermediate water hydrothermal plume. Geochimica et Cosmochimica Acta 69 (4), 933–952.

Buck, C.S., Landing, W.M., Resing, J.A., Lebon, G.T., 2006. Aerosol iron and aluminium solubility in the northwest Pacific Ocean: results from the 2002 IOC cruise. Geochemistry, Geophysics, Geosystems 7, Q04M07.

Byrne, R.H., Kim, K.-H., 1990. Rare earth element scavenging in seawater. Geochimica et Cosmochimica Acta 54, 2645–2656.

Charrassin, J.B., Park, Y.H., Le Maho, Y., Bost, C.A., 2004. Fine resolution 3D temperature fields off Kerguelen from instrumented penguins. Deep-Sea Research I 51 (12), 2091–2103.

De Baar, H.J.W., Baco, M.P., Brewer, P.G., 1983. Rare-earth distributions with a positive Ce anomaly in the Western North Atlantic Ocean. Nature 301, 324–327.

De Baar, H.J.W., Bacon, M.P., Brewer, P.G., Bruland, K.W., 1985. Rare-earth Elements in the Pacific and in the Atlantic Oceans. Geochimica et Cosmochimica Acta 49, 1953–1959.

De Baar, H.J.W., de Jong, J.T.M., Bakker, D.C.E., Löscher, B.M., Veth, C., Bathmann, U., Semetacek, V., 1995. Importance of iron for phytoplankton spring blooms and CO2 drawdown in the Southern Ocean. Nature 373, 412–415.

Doucet, S., Scoates, J.S., Weis, D., Giret, A., 2005. Constraining the components of the Kerguelen mantle plume: A Hf–Pb–Sr–Nd isotopic study of picrites and high-MgO basalts from the Kerguelen Archipelago. Geochemistry, Geophysics, Geosystems 6, Q04007.

Elderfield, H., Greaves, M.J., 1982. The rare earth elements in seawater. Nature 296, 214–219.

Elrod, V.A., Berelson, W.M., Coale, K.H., Johnson, K.S., 2004. The flux of iron from continental shelf sediments: a missing source for global budgets. Geophysical Research Letters 31 (12).

German, C.R., Masuzawa, T., Greaves, M.J., Elderfield, H., Edmond, J., 1995. Dissolved rare earth elements in the Southern Ocean: cerium oxidation and the influence of hydrography. Geochimica et Cosmochimica Acta 59, 1551–1558.

Gledhill, M., Van den Berg, C.M.G., 1994. Determination of complexation of iron (III) with natural organic complexing ligands in seawater using cathodic stripping voltammetry. Marine Chemistry 47, 41–54.

Goldstein, S.L., Hemming, S.R., 2003. Long lived isotopic tracers in oceanography, paleoceanography, and ice sheet dynamics. In: Elderfield, H. (Ed.), Treatise on Geochemistry—The Oceans and Marine Geochemistry, vol. 6. Elsevier, Amsterdam, pp. 453–489.

Haley, B.A., Klinkhammer, G.P., McManus, J., 2004. Rare earth elements in pore waters of marine sediments. Geochimica et Cosmochimica Acta 68 (6), 1265–1279.

Jacquet, S., Dehairs, F., Savoye, N., Obernosterer, I., Christaki, U., Monnin, C., Cardinal, D., 2008. Mesopelagic organic carbon remineralization in the Kerguelen Plateau region tracked by biogenic particulate Ba. Deep-Sea Research II, this issue [doi:10.1016/j.dsr2.2007.12.038].

Jeandel, C., Bishop, J.K., Zindler, A., 1995. Exchange of Nd and its isotopes between seawater small and large particles in the Sargasso Sea. Geochimica et Cosmochimica Acta 59, 535–547.

Jeandel, C., Ruiz-Pino, D., Gjata, E., Poisson, A., Brunet, C., Charriaud, E., Dehairs, F., Delille, D., Fiala, M., Fravalo, C., Miquel, J.C., Park, H.Y., Pondaven, P., Queguiner, B., Razouls, S., Shauer, B., Treguer, P., 1998a. KERFIX, a time-series station in the Southern Ocean: a presentation. Journal of Marine Systems 17 (1–4), 555–569.

Jeandel, C., Thouron, D., Fieux, M., 1998b. Concentrations and Isotopic compositions of Nd in the Eastern Indian Ocean and Indonesian Straits. Geochimica et Cosmochimica Acta 62, 2597–2607.

Johnson, K.S., Chavez, F.P., Friederich, G.E., 1999. Continental-shelf sediment as a primary source of iron for coastal phytoplankton. Nature 398 (6729), 697–700.

Kato, Y., Ohta, I., Tsunematsu, T., Watanabe, Y., Isozaki, Y., Maruyama, S., Imai, N., 1998. Rare earth element variations in mid-Archean banded iron formations: implications for the chemistry of ocean and continent and plate tectonics. Geochimica et Cosmochimica Acta 62 (21–22), 3475–3497.

Lacan, F., Jeandel, C., 2001. Tracing Papua New Guinea imprint on the central Equatorial Pacific Ocean using neodymium isotopic compositions and rare earth element patterns. Earth and Planetary Science Letters 186, 497–512.

Lacan, F., Jeandel, C., 2005. Neodymium isotopes as a new tool for quantifying exchange fluxes at the continent-ocean interface. Earth and Planetary Science Letters 232.

Marinov, I., Gnanadesikan, A., Toggweiler, J.R., 2006. The Southern Ocean biogeochemical divide. Nature 441 (7096), 964–967.

McCartney, M.S., Donohue, K.A., 2007. A deep cyclonic gyre in the Australian-Antarctic Basin. Progress in Oceanography, in press, doi:10.1016/j.pocean.2007.02.008.

Moffett, J.W., 1994. A radiotracer study of cerium and manganese uptake onto suspended particles in Chesapeake Bay. Geochimica et Cosmochimica Acta 58, 695–703.

Mongin, M., Molina, E., Trull, T., 2008. Seasonality and scale of the Kerguelen Plateau phytoplankton bloom: a remote sensing and modeling analysis if the influence of natural iron fertilization in the Southern Ocean. Deep-Sea Research II, this issue [doi:10.1016/j.dsr2.2007.12.039].

Moore, W.S., Krest, J., Taylor, G., Roggenstein, E., Joye, S., Lee, R., 2002. Thermal evidence of water exchange through a coastal aquifer: implications for nutrient fluxes. Geophysical Research Letters 29 (14).

Oelkers, E.H., Gislason, S.R., 2001. The mechanism, rates and consequences of basaltic glass dissolution: I. An experimental study of the dissolution rates of basaltic glass as a function of aqueous Al, Si and oxalic acid concentration at 25 °C and pH = 3 and 11. Geochimica et Cosmochimica Acta 65 (21), 3671–3681.

Park, Y.H., Charriaud, E., Fieux, M., 1998a. Thermohaline structure of the Antarctic Surface Water Winter Water in the Indian sector of the Southern Ocean. Journal of Marine Systems 17 (1–4), 5–23.

Park, Y.H., Charriaud, E., Pino, D.R., Jeandel, C., 1998b. Seasonal and interannual variability of the mixed layer properties and steric height at station KERFIX, southwest of Kerguelen. Journal of Marine Systems 17 (1–4), 571–586.

Park, Y.H., Fuda, J.L., Durand, I., Naveira Garabato, A.C., 2008a. Internal tides and vertical mixing over the Kerguelen Plateau. Deep-Sea Research II, this issue [doi:10.1016/j.dsr2.2007.12.027].

Park, Y.H., Roquet, F., Durand, I., Fuda, J.L., 2008b. Large scale circulation over and around the Northern Kerguelen Plateau. Deep-Sea Research II, this issue [doi:10.1016/j.dsr2.2007.12.030].

Roy-Barman, M., Chen, J.H., Wasserburg, G.J., 1996. $^{230}$Th–$^{232}$Th systematics in the Central Pacific Ocean: the sources and the fates of thorium. Earth and Planetary Science Letters 139, 351–363.

Rue, E.L., Bruland, K.W., 1997. The role of organic complexation on ambient iron chemistry in the equatorial Pacific Ocean and the response of a mesoscale iron addition experiment. Limnology and Oceanography 42 (5), 901–910.

Sholkovitz, E.R., Schneider, D.L., 1991. Cerium redox cycles and rare earth elements in the Sargasso Sea. Geochimica et Cosmochimica Acta 55, 2737–2743.

Sholkovitz, E.R., Shaw, T.J., Schneider, D.L., 1992. The geochemistry of rare earth elements in the seasonally anoxic water column and porewaters of Chesapeake Bay. Geochimica et Cosmochimica Acta 56, 3389–3402.

Sholkovitz, E.R., Landing, W.M., Lewis, B.L., 1994. Ocean particle chemistry: the fractionation of rare earth elements between suspended particles and seawater. Geochimica et Cosmochimica Acta 58, 1567–1579.

Sholkovitz, E.R., Elderfield, H., Szymczak, R., Casey, K., 1999. Island weathering: river sources of rare earth elements to the Western Pacific Ocean. Marine Chemistry 68, 39–57.

Tachikawa, K., Jeandel, C., Vangriesheim, A., Dupré, B., 1999. Distribution of rare earth elements and neodymium isotopes in suspended particles of the Tropical Atlantic Ocean (EUMELI site). Deep-Sea Research I 46, 733–756.

Taylor, S.R., McLennan, S.M., 1985. The Continental Crust. Its Composition and Evolution. An Examination of the Geological Record Preserved in Sedimentary Rock. Blackwell Publishing, Oxford.

van Beek, P., Bourquin, M., Reyss, J.L., Souhault, M., Charette, M. Jeandel, C., 2008. Radium isotopes to investigate the water mass pathways on the Kerguelen Plateau (Southern Ocean). Deep-Sea Research II, this issue [doi:10.1016/j.dsr2.2007.12.025].

Venchiarutti, C., Jeandel, C., Roy-Barman, M., 2008. Particle dynamic study in the wake of Kerguelen Island using thorium isotopes (Southern Ocean, KEOPS program). Deep-Sea Research I, submitted for publication.

Weis, D., Frey, F.A., Schlich, R., Schaming, M., Montigny, R., Damasceno, D., Mattielli, N., Nicolaysen, K.E., Scoates, J.S., 2002. Trace of the Kerguelen mantle plume: evidence from seamounts between the Kerguelen Archipelago and Heard Island, Indian Ocean. Geochemistry, Geophysics, Geosystems 3.

Yeghicheyan, D., Carignan, J., Valladon, M., Le Coz, M.B., Le Cornec, F., Castrec-Rouelle, M., Robert, M., Aquilina, L., Aubry, E., Churlaud, C., Dia, A., Deberdt, S., Dupr, B., Freydier, R., Gruau, G., Henin, O., de Kersabiec, A.M., Mace, J., Marin, L., Morin, N., Petitjean, P., Serrat, E., 2001. A compilation of silicon and thirty one trace elements measured in the natural river water reference material SLRS-4 (NRC-CNRC). Geostandards Newsletter—The Journal of Geostandards and Geoanalysis 25 (2–3), 465–474.